Università degli Studi di Padova

Department of Information Engineering

Master Thesis in ICT for Internet and Multimedia

Physical Layer Techniques to improve the performances of the LoRaWAN networks

Supervisor
Prof. Lorenzo Vangelista
Università di Padova

Master Candidate
Alessandro Cattapan

5 March 2020
Academic Year: 2019/2020

Abstract

The need of connecting more and more devices has given rise to the new communication paradigm of Internet of Things (IoT), which has rapidly gained ground in the last years. These devices, also called *things*, are objects from our everyday life equipped with a microcontroller, a transceiver, sensors and actuators that let them collect data from the environment, process the information and interact with each other in order to reach a common goal. All this is allowed by novel communication standards that are emerging with IoT. In particular, Low Power Wide Area Networks (LPWANs) are very appealing for their ability to provide long range communications and low power consumption in the license-free frequency bands. One of the most prominent LPWAN technology is LoRa, which will be the central topic of this thesis.

At first we will describe the LoRa modulation and the LoRaWAN networks. Then we will investigate the orthogonality between the signals used in the modulation, which will be exploited to introduce two new innovative techniques *DOLoRa* and *DLoRa* to improve the performances of the LoRaWAN networks. Finally, some evaluations at network level on these novel methods are carried out and reported through computer simulations.

Sommario

La necessità di connettere sempre più dispositivi ha dato origine al nuovo paradigma di comunicazione dell' Internet delle Cose (IoT), che negli ultimi anni ha acquisito molto terreno. Questi dispositivi, anche chiamati *things*, sono degli oggetti della vita comune equipaggiati con dei microcontrollori, dei transceiver, dei sensori e degli attuatori che permettono loro di raccogliere dati dall'ambiente esterno, processare le informazioni e comunicare tra loro al fine di raggiundere degli obiettivi comuni. Tutto questo è reso possibile dai nuovi protocolli di comunicazione che stanno emergendo con l' IoT. In particolare, le Low Power Wide Area Networks (LPWANs) sono molto allettanti per la loro capacità di fornire comunicazioni a lungo raggio e a basso consumo di energia sfruttando le bande di frequenza libere. Una delle tecnologie LPWAN più promettenti è LoRa, che sarà l'argomento centrale di questa tesi.

All'inizio descriveremo la modulazione LoRa e le reti LoRaWAN. Poi studieremo l'ortogonalità tra i segnali usati nella modulazione, ortogonalità che sarà sfruttata per introdurre due tecniche innovative *DOLoRa* e *DLoRa* per migliorare le prestazioni delle reti LoRaWAN. In conclusione saranno valutati i due nuovi metodi a livello di rete attraverso delle simulazioni al computer.

Contents

List of Figures

List of Tables

List of Acronyms

3GPP	3rd Generation Partnership Project
ABP	Activation By Personalization
ACK	Acknowledgement
ADR	Adaptive Data Rate
AES	Advance Encryption System
AS	Application Server
AWGN	Additive White Gaussian Noise
BER	Bit Error Rate
BPSK	Binary Phase Shift Keying
CIoT	Cellular IoT
CRC	Cyclic Redundancy Check
CSS	Chirp Spread Spectrum
DFT	Discrete Fourier Transform
DLoRa	Decreasing LoRa
DOLoRa	Dual Orthogonal LoRa
DSSS	Direct-Sequence Spread Spectrum
ED	End Devices
EIRP	Effective Isotropic Radiated Power
eNB	Evolved Node B
EPS	Evolved Packet System
ERP	Effective Radiated Power

ETSI	European Telecommunications Standards Institute
FEC	Forward Error Correction
FFT	Fast Fourier Transform
GW	Gateway
IEEE	Institute of Electrical and Electronics Engineers
IoT	Internet of Things
ISM	Industrial Scientific Medical
ITU	International Telecommunications Union
JS	Join Server
LPWAN	Low Power Wide Area Network
LTE	Long Term Evolution
MIC	Message Integrity Code
NB-IoT	Narrowband IoT
NS	Network Server
NS3	Network Simulator 3
OTAA	Over-The-Air Activation
PDU	Protocol Data Unit
PER	Packet Error Rate
PGW	Packet Data Network Gateway
PRB	Physical Resource Block
QPSK	Quadrature Phase Shift Keying
RAT	Radio Access Technology
RPMA	Random Phase Multiple Access
RPTDMA	Random Phase Time Division Multiple Access

SCEF	Service Capability Exposure Function
SDN	Software Defined Radio
SEM	Simulation Execution Manager
SF	Spreading Factor
SGW	Serving Gateway
SINR	Signal-to-noise-plus-interference ratio
SIR	Signal-to-interference ratio
SNR	Signal-to-noise ratio
SS	Spread Spectrum
ToA	Time On Air
UE	User Equipment
UNB	Ultra Narrowband
USRP	Universal Software Radio Peripheral

1 Introduction

Our life is more and more characterized by the proliferation of smart devices connected to the Internet, in particular in these years is gaining much more momentum the paradigm of Internet of Things (IoT). The basic idea behind this concept is the connection of things from our everyday life to the Internet [11] and the creation of a network of sensors and actuators blended seamlessly with the environment around us [12]. This paradigm finds application in different areas, such as industrial automation, smart homes, medical aids, mobile healthcare, environmental and domestic monitoring, waste management, structural analysis of old buildings or bridges to prevent their collapse, and many others [13]. Such diversity in the field of application makes very difficult to find a general solution that can fit every application and for this reason there are various architectures attempting to define the mode of operation of IoT devices. However, the most simple and efficient model can be defined by means of three entities as represented in Figure 1.1:

- *Backend Servers.* The central entity of the system is the backend server, which is responsible of storing and processing all the data collected in order to produce added-value services;
- *Gateways.* The role of the gateways is to interconnect the end devices (ED) with the servers. In particular they are also used to provide protocol translation between the unconstrained devices (servers) and the constrained

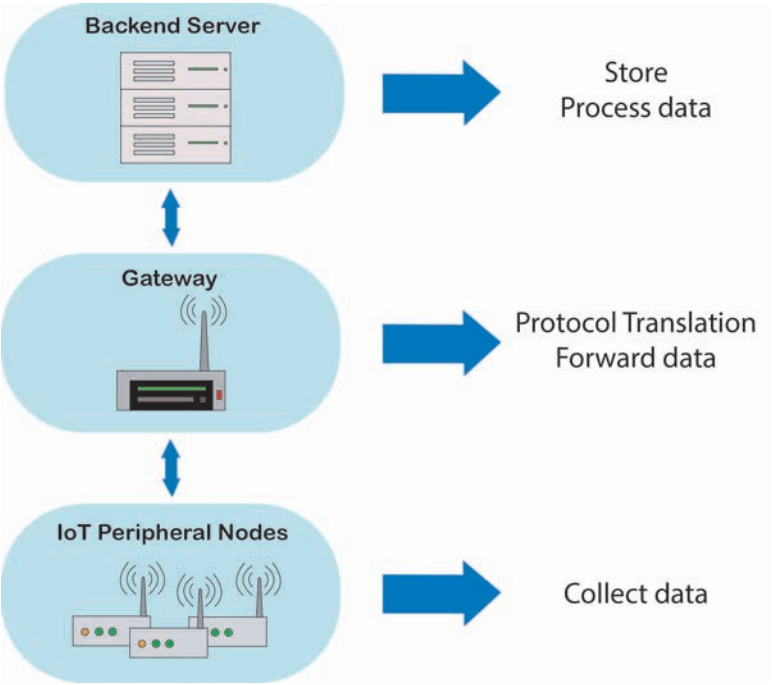

Figure 1.1: The Iot entities with their roles.

one (end devices);

- *Iot Peripheral Nodes*. At the edge of the network we have the devices in charge of collecting the data to deliver to the central server.

The new IoT paradigm implies the pervasive presence in our life of smart objects, which are constrained devices in the sense that they are subject to some limitations:

- **High scalability**: The number of IoT devices is projected to amount to 75.44 billion worldwide by 2025, which corresponds to a five hold increase in the last ten years [14]. The IoT networks should take into account this exponential growth and adopt all the necessary strategies in the physical layer and medium access control in order to support a very densely populated wireless environment while keeping the complexity of the systems low.
- **Low cost**: As we have anticipated the IoT networks will be pervasive, which means that it will be necessary to deploy an enormous quantity of devices. To make it affordable not only the devices should be cheap but also the necessary subscriptions cost to access the network should be low.
- **Limited power**: It is expected that lots of the devices will run on batteries,

and because of the dimensions of the networks it will be unmanageable to have a continuous maintenance of every node. So a common target for the battery life of the edge devices is in the order of 5 to 10 years, depending on the frequency of transmission.

- **Low bitrate**: IoT devices will not need to transmit data at high bitrate, but it is expected that they will send infrequently tiny amount of data. Furthermore it is usually preferred to have a resilient communication from/to devices, which can come at the expense of a low bitrate.
- **Good coverage**: The possibility to establish long range communications can have many beneficial effects. For example in the case of tracking devices a unique gateway can follow the displacement of a single node in a range of some kilometres without handling handovers, which then become less frequent. Moreover the ability to cover large areas has also the advantage to reduce the equipment required to build the network and then reduce the costs for the deployment.
- **Limited computational power**: As a consequence of all the previous requirements the computational complexity of the end devices will be very small. In fact their main aim will be only to collect data from the environment and send them to the server, which will be in charge of the real processing part.

In the last years, many solutions have been proposed to try to address these requirements. Mainly they are application specific solutions, in fact different application areas have specific constraints, which leads to the adoption of different technologies. The widely deployed short range radio connectivity (e.g, ZigBee) are not suitable for scenarios where long range communications and low power is needed. IoT solutions based on cellular technologies can be very good for the large coverage and low latency requirements, but they consume too much energy [15].

Low Power Wide Area Network (LPWAN) systems are targeting the massive Internet of Things market, and in the last years they are also getting quite a lot of traction. LPWAN is a new class of technologies that at the same time enables wide area communications and low power requirements.

The focus of this thesis will be one of the most prominent LPWAN technologies, LoRaWAN. Quite recently, there has been a rising interest on the physical layer

of LoRaWAN, i.e. the LoRa modulation, started by [1], continued by the letter [16], and then amended and improved by [17].

This work will present two improvements of the LoRa modulation called *Dual Orthogonal LoRa modulation* (DOLoRa) and *Decreasing LoRa* (DLoRa), which aim at solving the most highlighted problems for LoRaWAN networks i.e., the congestion and the scalability of LoRaWAN [7, 18]. In both the cases our target is reached with a cross-layer design framework [19]. The analysis is also supported by simulations using NS3 [20].

The thesis is organized as follows:

- Chapter 2 describes some of the most relevant LPWAN technologies that are currently available.
- Chapter 3 derives all the equations that describe the LoRa modulation and it focuses on the LoRa properties, that will be the basis of the two new modulations DOLoRa and DLoRa.
- Chapter 4 analyses the orthogonality between LoRa signals by means of MATLAB simulations. At the end of the chapter we will also get a quantitative way to describe the isolation between the waveforms.
- Chapter 5 provides a detailed description of the new innovative techniques: DOLoRa and DLoRa, that improve the performances of the LoRaWAN networks. The analysis will be accompanied to some simulations using NS3.
- Chapter 6 draws the conclusions of the thesis and identifies some possible ways for the future work on this topic.

2

Low Power Wide Area Network for IoT

Nowadays Low Power Wide Area Networks (LPWAN) are attracting a lot of interest for applications pertaining the massive Internet of Things, because of their peculiar ability to provide wide area communications at low power requirements. The low power consumption, which is in the order of 25 mW corresponds also to a lower complexity in the system implementation and to a longer battery life. Another appealing characteristic for this group of technologies is the large coverage area, whose range is in the order of 10-15 km in rural areas and 2-5 km in urban areas [3]. The downside of long-range systems is the low data rate, which usually ranges from few hundreds to few thousand bits per seconds. Even though this is not enough for data-hungry network applications, it surely suffices for smart cities scenarios, characterized by sporadic and intermittent transmissions of very tiny packets, in the order of few tens of bytes.

In this chapter we will analyse the main technologies associated to the LPWAN with a special focus on LoRa and LoRaWAN.

2.1 LPWAN technologies

LPWAN come into two flavours: one using licensed frequency bands and another using unlicensed frequency bands. NB-IoT and LoRaWAN are the two champions for each of the two type of bands, respectively [15]. Other standards that are

notable to be highlighted are SigFox and Ingenu, which will be described in the following sections.

2.1.1 NB-IoT

Narrowband IoT is a relatively new technology standardized by 3GPP [21] as a reaction of the telco operators to the growing market of IoT devices. Although it is part of the Release 13 [21] of the LTE standard, it can be seen as a separate wireless interface. Cost minimization and battery consumption are achieved by keeping the technology as simple as possible, and so many features of the LTE such as handover, carrier aggregation, measurement report and inter-RAT mobility are missing.

NB-IoT uses the same licensed frequency bands of the LTE, and is based on a QPSK modulation. It can be deployed in three different ways: stand-alone, guard band and in-band. In in-band and guard-band modes, NB-IoT occupies one Physical Resource Block [21] of 180 kHz in the LTE spectrum, while in the stand-alone version it occupies 200 kHz in the GSM spectrum [22]. This flexibility has allowed a fast integration of the service into the legacy LTE systems.

The architecture of the network is based on the evolved packet system (EPS) and on an optimization for cellular IoT (CIoT) of the user and control plane, as represented in Figure 2.1. The procedure to access the cell is almost equivalent to the one of LTE, where the evolved base station (eNB) handles the radio communication between the CIoT User Equipment (UE) and the Mobile Management Entity (MME). This allows the reuse of the existing LTE network architecture and backbone [15].

Another important characteristic of NB-IoT is the possible use of both IP and non-IP data traffic. The former is transmitted to the packet data network gateway (PGW) through the serving gateway (SGW). The latter is sent to a new entity, the service capability exposure function (SCEF) node, which can deliver user data piggybacked on the control data. Thanks to the user plane CIoT EPS optimization, both IP and non-IP data can be transmitted over the radio carriers via the SGW and PGW or via the MME and SCEF towards the application server. These two information paths can be implemented either one or both depending on the operator choice.

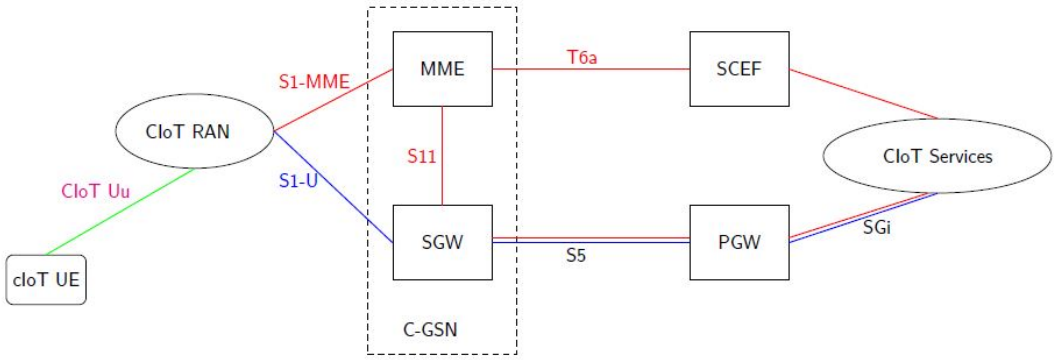

Figure 2.1: NB-IoT architecture.

2.1.2 SigFox

SigFox adopts the principle of Ultra Narrowband (UNB) communications with a BPSK modulation to transmit the packets over its network. Since it is an UNB technology the bandwidth occupied by any transmission is very small, only 100 Hz, and consequently the resulting bitrate is very low, in the order of 100 bps [1]. Devices access the wireless channel randomly in time and in frequency without sensing it before, which corresponds to an ALOHA-based protocol (Figure 2.2).

This brings some advantages i.e., nodes do not consume energy for the medium sensing, time synchronization is not needed and there is no constraint in the oscillator precision, because all frequencies inside the designed band are allowed. One of the most relevant disadvantages is the possibility to have packet collisions, which can happen with a very small probability since the transmission bandwidth is very small with respect to the available spectrum.

The demodulation is done by an efficient Software Defined Radio (SDR) that scans the entire spectrum by means of a FFT and then detects the packets sent. Therefore the response of the base station, if required, is sent on the same frequency of the received data. In that way the complexity of the end devices (ED) can be kept very low.

The reliability and robustness of the communication is achieved by sending up to three times the same packet in different frequency, and by employing the fre-

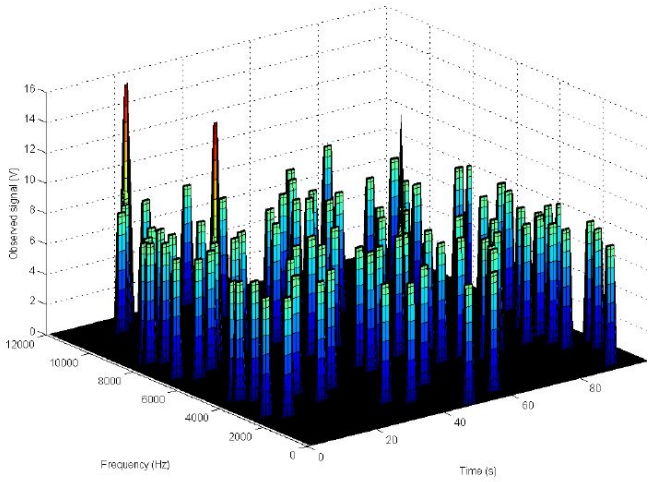

Figure 2.2: Example of temporal and spectral division of nodes in SigFox [1].

quency hopping technique, which consist in randomly changing the transmission frequency periodically.

Finally SigFox is very appealing for the very wide coverage area, which can reach 63 km in terrestrial communications, and for the low energy consumption during transmission that varies from 20 mA to 70 mA. But all this comes at the expense of the very little amount of data that can be transmitted inside every packet, whose maximum payload is made of only 12 bytes.

2.1.3 Ingenu

Random Phase Multiple Access (RPMA) is an innovative MAC technology developed by the American company On-Ramp Wireless, that in 2015 became Ingenu. Initially the company provided the connectivity only for the oil and gas applications, but in the recent years they extended their interest to the entire IoT market [1].

RPMA is based on Direct-Sequence Spread Spectrum (DSSS) techniques, in fact the data packet, after being encoded (1/2 rate) and interleaved, is spread with a Gold Code. Every time that we double the spreading factor of the Gold Code, which is equal to 2^k with $2 \leq k \leq 13$, we get a processing gain of 3 dB. This allows the adaptation of the communication to the actual channel conditions.

The transmissions take place in the 2.4 GHz ISM band and every time they use a unique Gold Code, which guarantees that only the intended receiver is able to recover the data sent.

The Random Multiple Access is performed in a slotted time domain, where every device selects first a slot and then a subslot, where it will transmit the data signal with a random delay. The combination of the random delay and the uniqueness of the Gold Code, which has a low autocorrelation function, guarantees that transmissions with different delays can be always recovered and then that do no interfere. Thus RPMA is a slotted ALOHA protocol.

Ingenu estimates that with this patented technique it is possible to have around 1000 uplink transmitting devices inside each time slot and that we can reach a coverage area of about 10 km [1].

2.2 LoRa

LoRa is a proprietary physical layer technology proposed and patented by Semtech Corporation [23], base on Chirp Spread Spectrum (CSS) modulation techniques. It operates in a non-licensed band below 1 GHz for long range communications. In this section we will describe in more detail LoRa and LoRaWAN.

2.2.1 Introduction to the LoRa Modulation

Spread Spectrum (SS) is a technique that increases the signal bandwidth beyond the minimum required to transmit the underlying data bits. At a first glance this can appear as a waste of resources, but the increase of the bandwidth can have some beneficial effects. It can attenuate the effects of inter-symbols and narrowband interference [24]. It can hide the signal below the noise floor and in fact these signals were originally used for military purposes [15]. Finally SS can provide multiple user access, because it allows the coexistence of more than one communication in the same time and the same space.

LoRa belongs to the family of Chirp Spread Spectrum (CSS) signals, which is a subcategory of Direct-Sequence Spread Spectrum (DSSS), a Spread Spectrum method. In particular, in DSSS, every symbol of the data signal is spread with a sequence of F chips (F is the so called *Spreading Factor*), whose values are in a

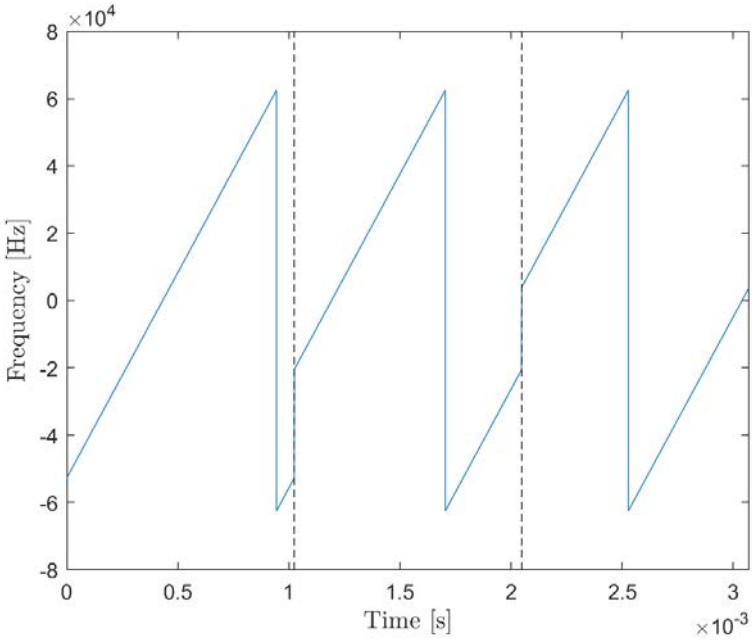

Figure 2.3: Plot of three Lora symbols with $SF = 7$.

finite set. The pattern of the chips sequence, used by the transmitter to encode the signal, is also used by the receiver to find the incoming signal [1].

In CSS modulation things change a little, in fact the sequence to spread the signal is obtained by means of a continuously varying carrier frequency and then chips lose their physical correspondence.

LoRa modulated signal is a passband signal of bandwidth B centred at the frequency $f_0 + \frac{B}{2}$, that corresponds to the 868 MHz band in Europe and to the 915 MHz band in USA. The actual LoRa signal occupies the frequencies in $\mathcal{B} = [f_0, f_0 + B]$. A LoRa signal is created so that it increases linearly in frequency from a starting frequency $f_s \in \mathcal{B}$ to that same frequency, wrapping around from $f_0 + B$ to f_0 when hitting the end of the available band, as we can see in Figure 2.3.

LoRa is an M-ary digital modulation, whose waveforms are not orthogonal and this will be better investigated in the next chapter. The number of available symbols and then the number of different waveforms M, depends on the selected

spreading factor SF, according to the following equation

$$M = 2^{SF} \tag{2.1}$$

Despite the Spreading Factor, which also corresponds to the number of bits encoded in every symbol, normally ranges from 5 to 12, in LoRaWAN is limited from 7 to 12. A transmission spreading factor is also used to determine the duration of the symbols

$$T_s = \frac{2^{SF}}{B} \tag{2.2}$$

We can notice that an increase of the spreading factor by only one unit yields to a double symbol duration. At the same time if we double the bandwidth we will also double the bitrate. An increasing transmission time for a chirp i.e, a symbol, is beneficial in term of robustness to interference or noise during the communication. Its counterpart is that transmitting longer messages increase the probability of collisions and the consumed energy.

As a consequence of all the previous argumentation it should be clear that the SF affects the receiver sensitivity, that is

$$S = -174 + 10\log_{10}(B) + NF + SNR_m \quad [dB] \tag{2.3}$$

where the first term derives from the thermal noise in 1 Hz of bandwidth and can only be influenced by changing the receiver noise temperature. NF is the noise figure of the circuitry at the receiver side and SNR_m is the minimum signal to noise ratio of the underlying modulation scheme required for a correct demodulation. Finally we can easily compute the bitrate of every spreading factor using (2.2):

$$R_b = \frac{SF}{T_s} \tag{2.4}$$

The bitrates for different spreading factors and different bandwidth are summarized in Table 2.1.

2.2.2 LoRa packet format and Time on Air

In order to increase the resiliency of the signal over the air, LoRa adopts a sequence of operations to implement before the modulation and the actual trans-

SF	125 kHz	250 kHz	500 kHz
7	6835	13671	27343
8	3906	7812	15625
9	2197	4396	8793
10	1220	2441	4882
11	671	1342	2685
12	366	732	1464

Table 2.1: Bitrate [bits/s] for various spreading factors and bandwidths.

mission:

- **Data whitening** is used to introduce randomness into the transmitted symbols and so keep the data Direct Current-free as specified in [2]. Then the received symbols will be de-whitened by XORing them with the same sequence used in the transmission [6].
- **Forward Error Correction (FEC)** enables the correction of wrongly received bits, without requiring the retransmission of the entire frame. LoRa uses an Hamming Code, whose codewords have length $4 + CR$, with $CR \in \{1, 2, 3, 4\}$. The information bits per codeword is fixed to 4 bits and so the variable coding rates are $\mathcal{C} \in \{4/5, 4/6, 4/7, 4/8\}$.
- **Interleaving** reshaffles the encoded bits in order to make the data packet more robust against bursty errors. The sequence of bits is stacked together in such a way to build a binary matrix $\mathcal{M} = \{0, 1\}^{SF \times (4+CR)}$, that is used to diagonally interleave the sequence [25].
- **Gray mapping** is used before transmitting the packet on air. It associates groups of SF bits to one of the M symbols available under the constraint that two adjacent symbols differ by only one bit.

The Physical layer LoRa packet comprises several elements, as shown in Figure 2.4. Now we can compute the Time on Air (ToA) with the following formula:

$$t_{packet} = t_{preamble} + t_{payload} \tag{2.5}$$

where $t_{preamble}$ is the time needed to transmit the preamble, and $t_{payload}$ is the time to transmit the information data. Therefore we can further express these

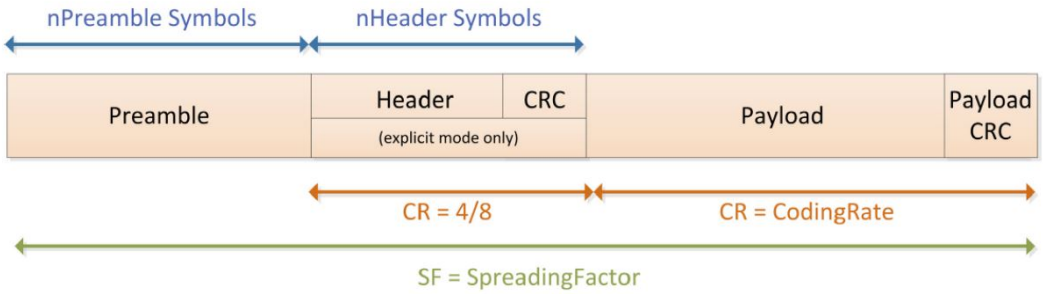

Figure 2.4: LoRa Physical layer packet formatting [2].

two quantities as:

$$t_{preamble} = (n_{preamble} + 4.25) \cdot T_s \tag{2.6}$$

$$t_{payload} = n_{payload} \cdot T_s \tag{2.7}$$

The first expression depends on $n_{preamble}$, which is a configurable parameter that affects the number of symbols in the preamble. The higher is that number and much probable will be the detection of the packets by the receiver. In the preamble there are always two modulated chirps, that are used for the frame synchronization, and two consecutive downchirps followed by a third downchirp of duration $T_s/4$, that are needed for the frequency synchronization [25]. All these symbols together form the fixed term 4.25 in the previous formula.

In the second expression (2.7) we have $n_{payload}$, whose definition is much more complicated. It depends on the following parameters [2, 26]:

- PL is the number of bytes in the payload.
- H can be either 0 or 1 depending on the packet header if it is respectively set to enabled or disabled. The header carriers information about the length of the payload. The default value is 0.
- DE is equal to 0 when the data rate optimization is disabled, otherwise it is set to 1. This mode consist in deleting the top two rows of the interleaving matrix, because they are more prone to errors. Therefore, in the data rate optimization mode, a reduced data rate is traded for an increased robustness to noise. The Lora PHY layer header is always transmitted in reduced rate mode, whereas the payload bytes are transmitted in that mode only if they

use $SF = 11$ or $SF = 12$ [25].
- CRC is set to 1 when the CRC field is present, or 0 when it is not.
- CR is the previously defined coding rate that goes from 1 to 4.

Given the above parameters the number of payload symbols is equal to

$$n_{payload} = 8 + \max\left(\left\lceil \frac{8PL - 4SF + 28 + 16CRC - 20H}{4(SF - 2DE)} \right\rceil (CR + 4), 0\right) \quad (2.8)$$

2.2.3 Properties of LoRa

Here we introduce the description of the *pseudo-orthogonality* of the spreading factors and the *channel capture* effect, that will be investigated more in depth in Chapter 4.

The Lora spreading factors are pseudo-orthogonal [27, 1], which means that two overlapping transmissions with different spreading factor sharing the same frequency channel, can be both successfully detected and demodulted at the receiver under certain conditions. These conditions are usually quantified in literature as a threshold in the power difference (in the logarithmic domain) between the two signals. For example Goursaud in [1] quantifies these threshold in terms of Signal-to-noise-plus-interference ratio (SINR), while Croce in [27] does a similar things in terms of Signal-to-interference ratio.

The *channel capture* effect instead regards signal with the same SF. If at the gateway (GW) there are two colliding packets with the same SF, it might be possible to recover the strongest signal if the power difference of the two signals is higher than a certain threshold [28]. These critical values can be computed in the same way of the previous thresholds for the spreading factors pseudo-orthogonality.

The beneficial effects of *channel capture* and SF *pseudo-orthogonality* make the performances of LoRa better than a simple ALOHA network, even though the medium access strategy is the same. The reason is that in a typical ALOHA network two interfering packets are always lost, while in LoRa, under certain power requirements, one or even both packets can survive.

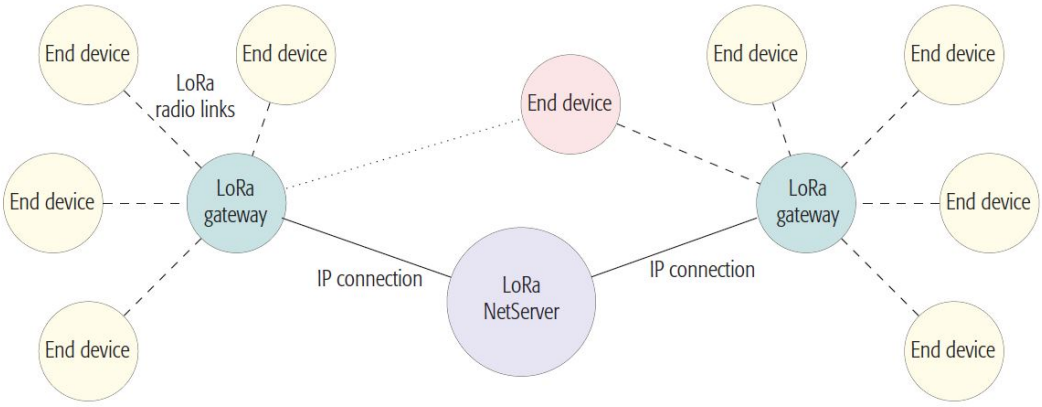

Figure 2.5: LoRa systems architecture [3].

2.3 LoRaWAN

Above the proprietary physical layer LoRa, there is the network layer protocol LoRaWAN, that is described in [4] by the LoRa Alliance, a non-profit association of companies committed to develop and maintain the LoRaWAN open standard. In this section we will report the main features of LoRaWAN, that will be needed for the analysis of the next Chapters.

2.3.1 Network Topology and Devices

The LoRaWAN network are usually deployed in a *star-of-star* topology [3] as represented in Figure 2.5, where the EDs are connected trough a single-hope LoRa link to one or many GWs, which, in turn, are connected to a common Network Server (NS) by means of standard IP protocol. The GWs act as simple packet forwarders between the EDs and the NS (Figure 2.6). The GW demodulates all the LoRa messages and then send them to the NS, after adding to the packet some control information about the quality of reception. The EDs are not required to associate to a unique GW, as normally happens in cellular networks, but only to the NS, which is then in charge to filter all the packets received and possibly delete duplicated or undesired packets. This architecture simplifies the access procedure to the network with obvious advantages for the end nodes, moving the complexity towards the NS. Moreover the communication between EDs and GWs is held on different frequency channels and at different data rates. To jointly minimize the

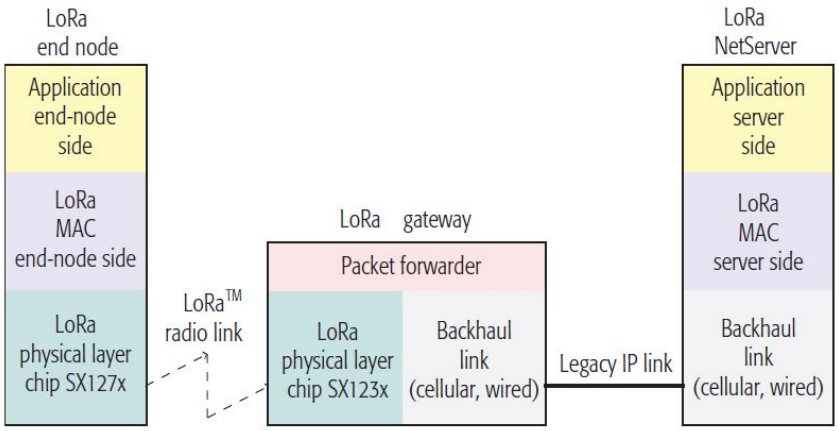

Figure 2.6: LoRa protocol architecture [3].

energy consumption of the EDs and maximize the overall network capacity, the LoRa systems are able to manage the data rate and the radio frequencies for the transmissions of every ED through an adaptive data rate (ADR) algorithm.

The LoRaWAN standards specifies three possible models for the behaviour of LoRa nodes:

- *Class A* (for *All*) defines the default functionality of nodes and must be mandatorily implemented by all LoRa devices. The EDs belonging to that class instantiate the communication with the NS in a total asynchronous way. After transmitting every packet they open two receive windows, one in the same frequency band of the uplink transmission, and the other on a different channel, previously agreed on with the NS. The change of the sub-channel for the second reception window is done to increase the resilience against channel fluctuations. Class A provides the lowest energy consumption for the nodes, but at the cost of possible long delays for the downlink, since it is always the ED that starts the communication and never the NS.
- *Class B* (for *Beacon*) is characterized by a synchronized communication between the EDs and the NS, thanks to the beacon packets broadcasted by Class B Gateways. The beacon mechanism allows a bidirectional communication between the NS and EDs irrespective of the uplink traffic. In fact the EDs can always receive downlink messages inside a specific time window. This class targets all the LoRa nodes that need to receive commands

or messages from the NS, e.g., actuators or switches.

- *Class C* (for *Continuously listening*) is intended for devices that do not have strict energy consumption limitations, generally for devices that are connected to the power grid, which can keep the reception window always open, except when they transmit. As a consequence this class is the optimal choice for devices that have strong delay requirements.

From now on during the thesis, if not explicitly states, we will always refer to the most common Class A, which is the most interesting for the typical IoT scenario.

2.3.2 MAC Packet Structure

The LoRaWAN specifications in [4] are not limited to the topology of the network and to the classes of devices, but they also describes the communication protocol. This includes the composition of PHY and MAC layer packets, the set of network parameters, like the SF and channel frequencies used by EDs, and the MAC commands. In Figure 2.7 we can see the packet structure of a LoRaWAN message, in particular the physical layer packet structure was already discussed in Section 2.2.2.

Inside the PHY payload we find the MAC protocol data unit (PDU), that is composed by a MAC header, followed by a MAC payload, and ending with a message integrity code (MIC). The MAC header specifies the message type and the major version of the LoRaWAN standard used by the end device. The possible message types with their description are summarized in Table 2.2.

The MAC payload contains a Frame header, a Frame port and a Frame payload. The Frame payload typically contains the data coming from the Application Layer, and the Frame Port is used to identify which application is the final receiver. The Frame header, instead, is composed by various parts that are connected to some aspects of the LoRa network. At first we have the short device address, which is used to identify the devices in a network. Then there is the Frame Control field, that is in charge of transporting the Acknowledgement (ACK) and the Frame pending bits. Finally there are two bits that are reserved for the ADR mechanism. In fact the NS, after the analysis of the control information added to the packets by the GW about the reception quality, has the ability to change

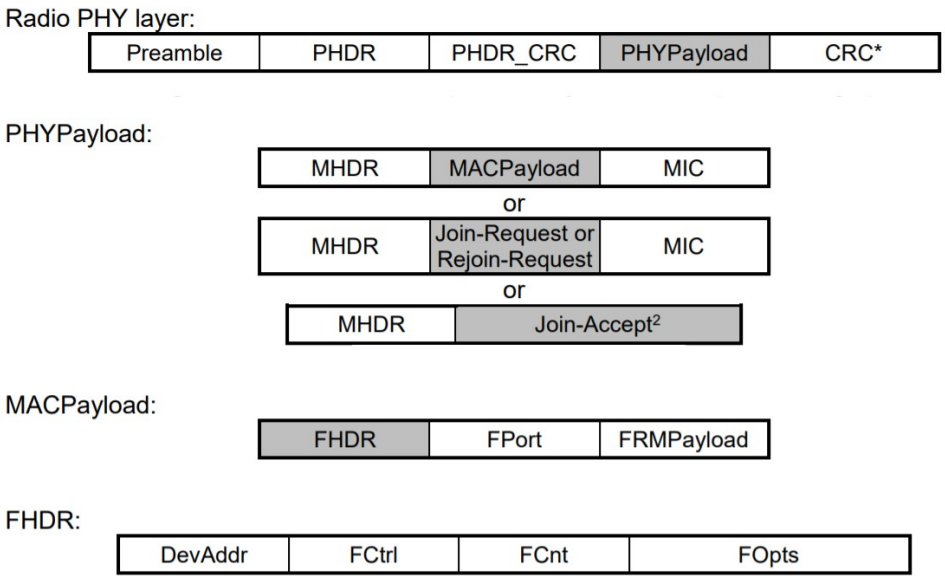

Figure 2.7: LoRaWAN packet structure [4].

Message Type	Description
000	Join-request
001	Join-accept
010	Unconfirmed Data Up
011	Unconfirmed Data Down
100	Confirmed Data Up
101	Confirmed Data Down
110	Rejoin-request
111	Proprietary

Table 2.2: MAC message types.

the node's spreading factor or to adjust its transmitting power. For example the ADR algorithm may choose to increase the SF of one ED with a low SNR, or it may also decide to decrease the SF of a device, whose packets are received with an high SNR. This last device will save energy while keeping active and reliable its communication with the GW. In other words, the ADR algorithm is used to guarantee the reliability of every device communication (by increasing the SF) while minimizing the ToA of the device's packets (by lowering the SF) and then consume less energy and avoid collisions. It is important to notice that the ADR mechanism is not standardized and in literature we can find various solutions, that have to face the trade-off between complexity and efficiency.

2.3.3 Devices Activation

For this section we need to take into consideration the LoRaWAN architecture scheme in Figure 2.8, which shows a more detailed description of the network backend. Now the NS is splitted in three different entities: the home NS, that store all the session information of the ED; the serving NS, which controls the MAC layer of the ED; and the forwarding NS, that manages the radio gateways [5]. Moreover there is a new element in the network, the Join Server (JS), which is responsible for the join procedure and the related key derivations of the EDs during the activation process.

Before taking part to a LoRaWAN network, every LoRa device has to be personalized and activated. The activation can be achieved in two ways, either via Over-The-Air Activation (OTAA) or via Activation By Personalization (ABP). In both the cases the activation relies on a set of keys, that are also used to encrypt the communications. Before describing the complex OTAA procedure, we need to list all the required elements, that must be securely stored inside the EDs before the join process:

- *JoinEUI* is a global application ID in the IEEE UUI64 address space, that univocally identifies the JS.
- *DevEUI* is a global device ID in the IEEE UUI64 address space, that allows all the NSs to uniquely identify the ED. This attribute is also recommended to be store in the ABP-only devices, even though it is not need for the activation process.

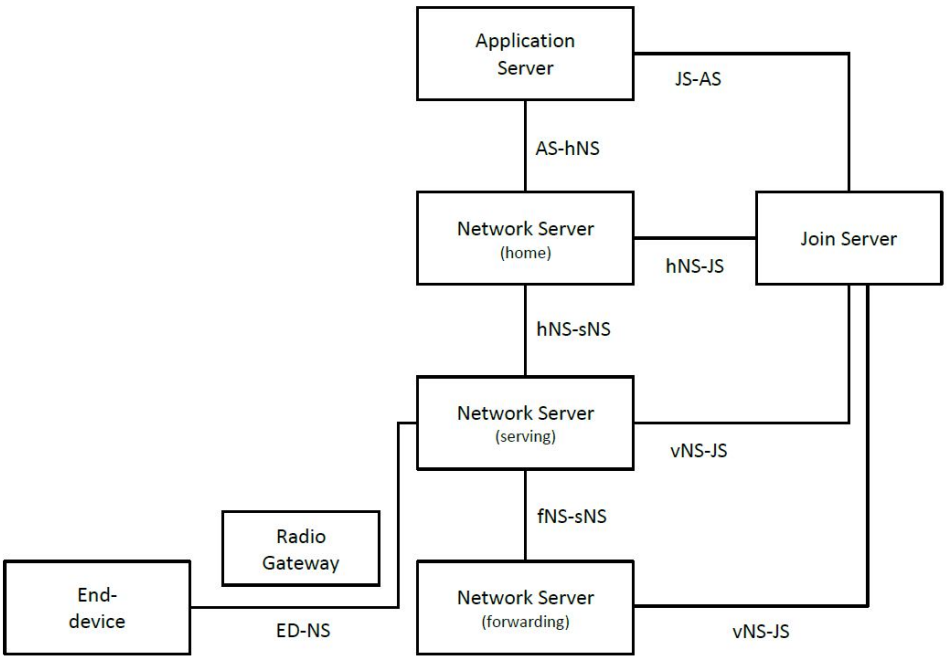

Figure 2.8: LoRaWAN architecture, with a detailed representation of the network Backend part [5].

- *NwkKey* is an AES-128 root key, that must be stored into the device during fabrication. Whenever an ED joins the network via OTAA, this key is used to derive the session keys as depicted in Figure 2.9. It is important to notice that there is a different procedure to generate the session keys with respect to the LoRaWAN version used. In fact in LoRaWAN 1.0 is required only the NwkKey from which is created the AppSKey and another key used, at the same time, as FNwkSIntKey, SNwkSIntKey and NwkSEncKey.
- *AppKey* is an AES-128 root key, that must be stored into the device during fabrication. It is used from the LoRaWAN version 1.1 to compute the AppSKey.

Both the NwkKey and the AppKey must be securely stored in the ED and also in the backend.

Once we get all these elements we are ready for the OTAA, which is a join procedure needed before the ED can take part to the data exchange with the NS. At first the device has to generate two lifetime keys starting from the NwkKey: the JSIntKey, that will be used for the MIC of the Rejoin-Request and the Join-

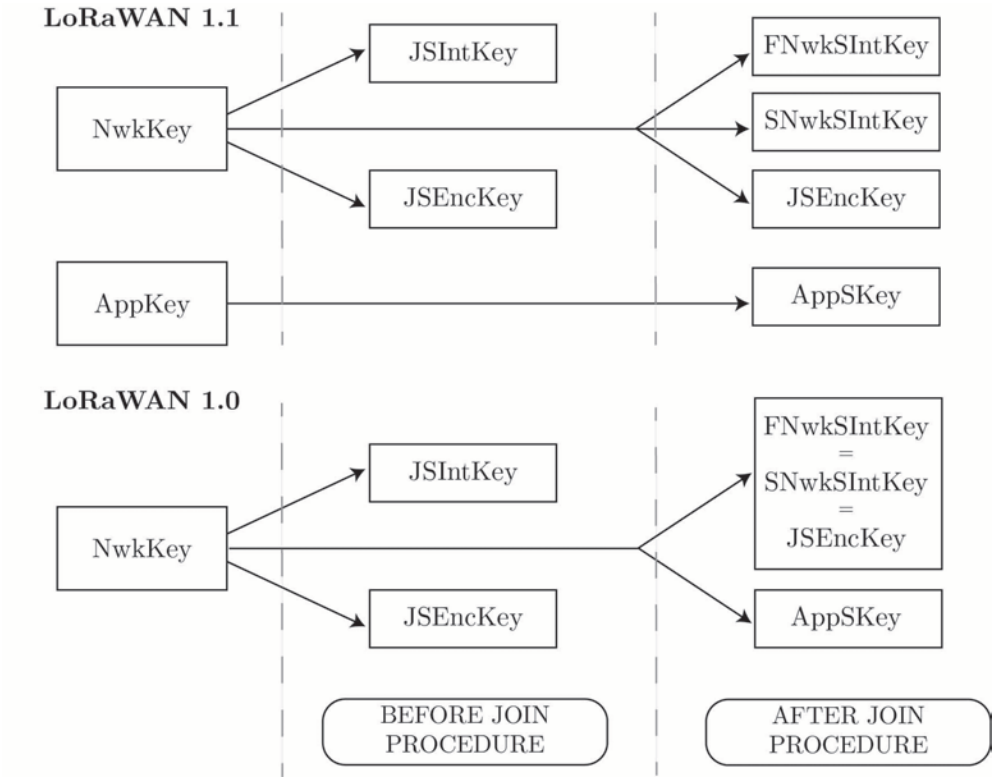

Figure 2.9: LoRaWAN keys derivation.

Accept answers; and the JSEncKey, which is used to encrypt the Join-Accept triggered by a Rejion-Request. Then it will send a Join-Request or a Rejoin-Request message, containing the DevEUI and the JoinEUI not encrypted.

The NS will respond with a Join-Accept if all the checks have a positive result, containing the network ID, the device address (used to identify the ED inside the network) and the JoinNonce, which is the most important piece of the message. In fact the JoinNonce is the missing part needed by the ED to build all the session keys for the communication: FNwkSIntKey, SNwkSIntKey, NwkSEncKey and AppSKey.

No response is given to the end-device if the Join-Request is not accepted by the NS.

After the activation the network session, which must be maintained by both the ED and the NS, and the application session, that must be kept by the ED and the Application Server (AS), are ready to be used. The network session context is composed by:

- FNwkSIntKey, the Forwarding Network Session Integrity Key, that is used to compute part of the MIC in the uplink traffic;
- SNwkSIntKey, the Serving Network Session Integrity Key, that is used to compute part of the MIC for the uplink communications and to verify the message integrity of the downlink traffic;
- NwkSEncKey, the Network Session Encryption Key, used to encrypt and decrypt uplink and downlink MAC commands (transmitted as payload) on the port 0;
- FCntDwn (LoRaWAN 1.0) or NFCntDown (LoRaWAN 1.1), the downlink frame counters;
- DevAddr, the address used to identify the device inside the network.

While the application session context is formed by:

- AppSKey, the application session key;
- FCntUp, the counter for the uplink frames;
- FCntDown (LoRaWAN 1.0) or AFCntDown (LoRaWAN 1.1), the downlink frame counters;

The Activation By Personalization (ABP) is much more easier to describe, but it is less flexible. In fact it ties an ED to a specific network by-passing all the previous join procedure. Activating a LoRa device though ABP means

Region	Frequency band (MHz)
Europe (EU)	863 - 870 and 433
United State (US)	902 - 928
China (CN)	779 - 787 and 470 - 510
Australia (AU)	915 - 928
Asia (AS)	470 - 510
South Korea (KR)	920 - 923
India (INDIA)	865 - 867

Table 2.3: Frequency bands of every region [8].

that we need to store the DevAddr and all the four session keys: FNwkSIntKey, SNwkSIntKey, NwkSEncKey and AppSKey directly on the node. Therefore the devices activated with this method are ready to take part to a specific LoRaWAN network as soon as they start the communication.

Finally, since all EDs are equipped with unique application and network root keys specific for each device, if a malicious users manages to extract the AppKey/NwkKey pair from one LoRa device, he compromises only the security of that single device and not the security of the entire system.

2.3.4 LoRaWAN Regional Parameters

The LoRa Alliance has reported in a separate document [8] from the one of LoRaWAN Specification, the LoRaWAN parameters set up for every specific region in the world. This is due to the fact that the ISM band are not allocated in the same part of the spectrum all over the countries and moreover the free frequency bands are subject to different regulations. In Table 2.3 are summarized the ISM bands for every region. In this section we will limit our discussion to the European ISM bands, whose regulations can reduce the performances of the LoRaWAN network as it is demonstrated in [7].

The ISM bands belongs to the unlicensed part of the spectrum, but this doesn't mean that everyone can use them freely, but these bands are subject to the regulations of the National Administrators, of the European organisms (e.g. CEPT and ETSI) and of the International Telecommunication Union (ITU), that operates at worldwide level. In Europe LoRa systems are subject to the European Conference of Postal and Telecommunications Administrations (CEPT) and to the European

Data Rate	Configuration	Indicative PHY bitrate [bit/s]
DR0	LoRa SF 12	250
DR1	LoRa SF 11	440
DR2	LoRa SF 10	980
DR3	LoRa SF 9	1760
DR4	LoRa SF 8	3125
DR5	LoRa SF 7	5470

Table 2.4: Data rate for EU ISM bands with bandwidth of 125 kHz [8].

f	B [kHz]	% of ToA	Max ERP [dBm]
868.1	125	1%	14
868.3	125	1%	14
868.5	125	1%	14
868.85	125	0.1%	14
869.05	125	0.1%	14
869.525	125	10%	27

Table 2.5: ISM band LoRa limitations according to ETSI regulations.

Telecommunications Standards Institute (ETSI) regulations that are collected in [29, 30]. The restriction are about the access of the physical channel, for example there are a limitations on the maximum transmission time or on the maximum transmission power.

Devices that wants to transmit in the ISM bands are required to either implement a listen before talk (LBT) policy or a duty cycle transmission, in order to give to all the users the same chances to use the physical medium. The duty cycle is defined as the allowed percentage of transmission time per hour, which means that if the duty cycle constraint is 1%, one device can transmit data for a maximum of 36 s per hour.

The policy adopted by LoRa is the one of the duty cycle, because for IoT devices it is important to keep their complexity as low as possible in such a way to reduce their energy consumption. This can affect more the generation rate of packets with high SF, to which corresponds a possible high ToA.

As anticipated, ETSI and CEPT impose also some limit in the maximum ir-

radiated power by the devices. These limits are expressed in terms of Effective Radiated Power (ERP), that is the power needed by an half-wave dipole to reach the same field strength that the tested device produces at the same distance. This quantity can be related to the Effective Isotropic Radiated Power (EIRP), which is defined in the same way of the ERP with the only difference to use an isotropic antenna instead of the half-wave dipole, by

$$ERP_{dBm} = EIRP_{dBm} - 2.15 \tag{2.9}$$

where 2.15 dBi is the maximum half-wave dipole gain with respect to the isotropic antenna. Since that the EIRP is defined as:

$$EIRP_{dBm} = 10 \log_{10} \left(\frac{E^2 \cdot r^2}{0.03} \right) \tag{2.10}$$

where E is the electrical field strength at the distance r from the transmitting antenna. We can now have a closed form to relate the actual electrical field strength to the ERP.

In the LoRaWAN Regional Specifications [8] there is a list of all the allowed transmission powers of the devices, and it also reports the values of reachable bitrates using the EU ISM bands (Table 2.4). Finally in Table 2.5 we summarize all the limits, in terms of power and duty cycle transmission time, imposed by ETSI for the European ISM bands.

3

LoRa Modulation

The LoRa modulation was originally introduced by Semtech with the US patent [23], that didn't provide an analytical description of the underlying equations. In literature the first study of the LoRa waveform's formulas can be found in [16], where there is a little inconsistency with the signal bandwidth that is two times the one desired. This article is very important because it triggered a sequence of papers on the LoRa signals, that terminated with [17], which amended and improved the original work of Vangelista.

An example of LoRa packet in the frequency domain can be seen in Figure 3.1 and 3.2, where on the vertical axis there are the frequencies and on the horizontal

Figure 3.1: Spectrogram of a LoRa packet [6].

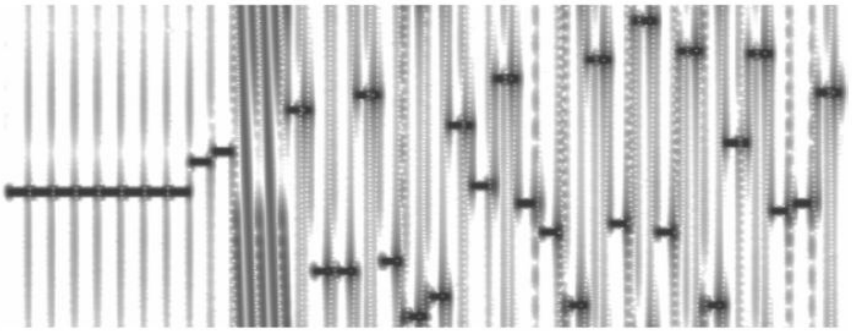

Figure 3.2: Spectrogram of a dechirped LoRa packet [6].

axis there is the time. In the first image is represented a simple LoRa packet, while in the second one, there is the corresponding dechirped version of the same packet.

This chapter will analyse the procedure to obtain the equations of the LoRa signals both in the continuous and in the discrete domain, because the same computations will be reused to build the new modulations in Chapter 5. Finally there will be the description of the LoRa modulation properties and of the demodulation process for the LoRa systems.

3.1 Equations in continuous and discrete time domain

Throughout this thesis we will use $u(t)$ to indicate the unit step function, and with $g_T(t)$ we will refer to the indicator function, which is equal to one for $0 \leq t \leq T$ and zero for the other values.

The mathematical description of the LoRa signal in the continuous domain is derived starting from the instantaneous frequency. The fact that the frequency linearly increase until it wraps back to the lower part of the band, when it hits the upper bound of the channel bandwidth, can be seen as a reduction modulo B.

For sake of clarity from now on we will consider the LoRa signal sweeping the frequencies in the interval $[0, B]$ as Figure in 3.3. Therefore in the time interval $t \in [0, T_s[$ and for the symbol $a \in \{0, 1, 2, ..., M-1\}$ the LoRa instantaneous

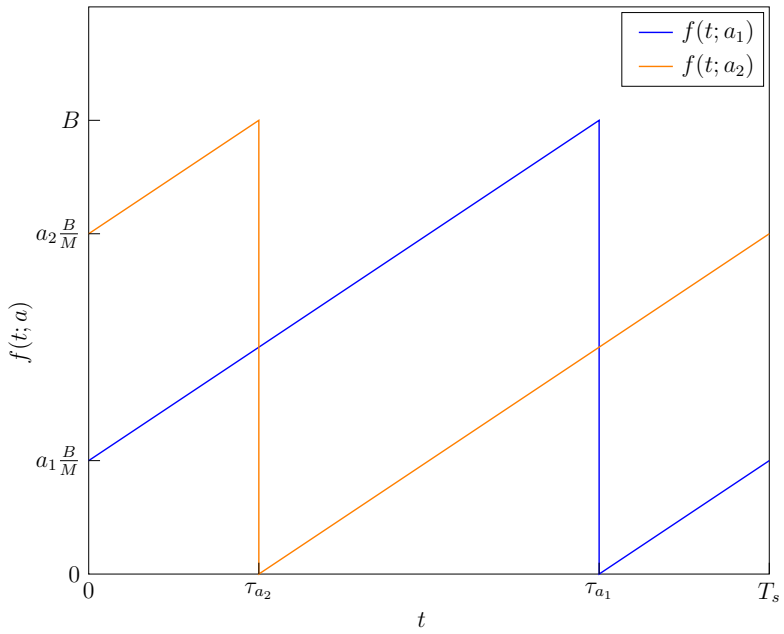

Figure 3.3: Instantaneous frequency $f(t;a)$ of two LoRa signals with symbols a_1 and a_2.

frequency can be written as

$$\begin{aligned} f(t;a) &= a\frac{B}{M} + \frac{B}{T_s}t \pmod{B} \\ &= a\frac{B}{M} + \frac{B}{T_s}t - Bu(t-\tau_a), \qquad 0 \leq t < T_s \end{aligned} \tag{3.1}$$

where aB/M is the initial frequency and

$$\tau_a = T_s\left(1 - \frac{a}{M}\right) \tag{3.2}$$

is the time instant, in which the signal reaches the maximum frequency B and then wraps back to 0. As anticipated before, this characteristic can be obtained by means of a modulo B operation. At this point, if we assume that the signal starts at $t = 0$, we can obtain its phase $\Phi(t;a)$ through the integration of the

instantaneous frequency in (3.1)

$$\begin{aligned}\phi(t;a) &= 2\pi \int_0^t f(\tau;a)d\tau \\ &= 2\pi \left[a\frac{B}{M}t + \frac{B}{2T_s}t^2 - B(t-\tau_a)u(t-\tau_a) \right]\end{aligned} \tag{3.3}$$

where during the computation of the final result it is possible to remove the term $B\tau_a = M - a$, because it is an integer and in the phase is multiplied by 2π.

Here we can remark that the main contribution of Chiani with [17] is the introduction of the factor $1/2$ before the quadratic term in the LoRa phase equations, which is missing in all the previous papers [16, 31].

The complex envelope of the LoRa modulated signal is

$$x_s(t;a) = \sqrt{2P_s}\exp\{j\phi(t;a)\}, \qquad 0 \le t < T_s \tag{3.4}$$

where P_s is the passband signal power. From now on, if not differently states, we will assume $P_s = 1$.

Usually it is preferred to describe the LoRa signal within the frequency interval $\left[-\frac{B}{2}, \frac{B}{2}\right]$, in such a way to have the signal band centred in zero and then have its base-band representation. This can be done by repeating all the previous steps with the only difference to add the term $-\frac{B}{2}$ in the instantaneous frequency

$$f(t;a) = a\frac{B}{M} + \frac{B}{T_s}t - Bu(t-\tau_a) - \frac{B}{2}, \qquad 0 \le t < T_s \tag{3.5}$$

that integrated will give us the desired formula

$$\begin{aligned}x(t;a) &= \exp\left\{ \jmath 2\pi \left[\frac{a}{M}Bt - \frac{1}{2}Bt + \frac{B^2t^2}{2M} - B(t-\tau_a)u(t-\tau_a) \right] \right\} \\ &= \exp\left\{ \jmath 2\pi Bt \left[\frac{a}{M} - \frac{1}{2} + \frac{Bt}{2M} - u\left(t - \frac{M-a}{B} \right) \right] \right\}, \qquad 0 \le t < T_s\end{aligned} \tag{3.6}$$

The last equality holds for the previous consideration that the term $B\tau_a = M - a$ is an integer number. In general we can write the complex envelope of a LoRa

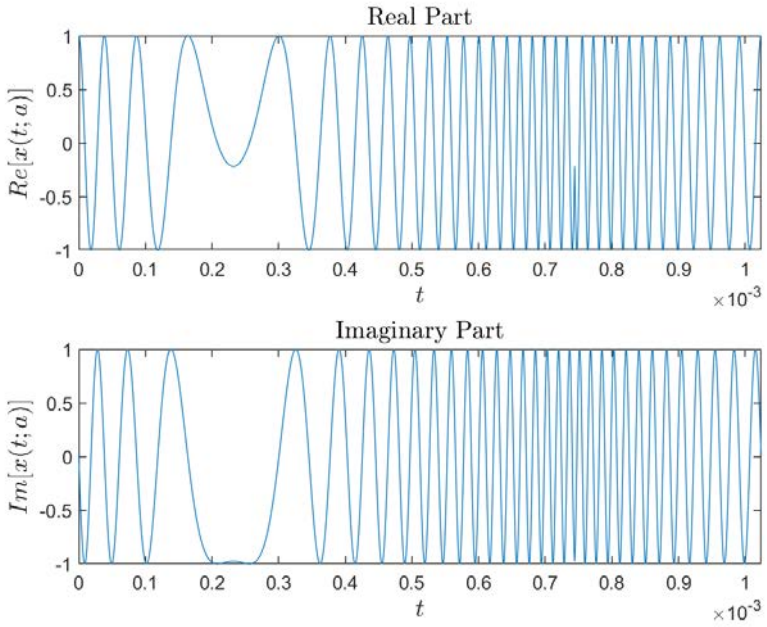

Figure 3.4: Plot of the real and imaginary part of a LoRa signal $x(t;a)$ with $a = 35, B = 125kHz$ and $SF = 7$.

signal as

$$v(t) = \sum_{n=-\infty}^{\infty} x(t - nT_s; a_n) g_{T_s}(t - nT_s) \tag{3.7}$$

where a_n is the symbol transmitted in the time interval $[nT_s, (n+1)T_s]$. Therefore the passband modulated signal centred in f_c is $s(t) = \mathfrak{Re}\{v(t) \cdot e^{j2\pi f_c t}\}$.

In Figure 3.4 and Figure 3.5 we can see the plot of a LoRa signal in the continuous time domain created by means of (3.5).

The LoRa receiver will get the discrete version of the signal, which according to [23], will be sampled every $T = \frac{1}{B} = \frac{T_s}{M}$ seconds. So the discrete equation in the interval $[0, T_s[$ is

$$\begin{aligned} x(kT; a) &= \exp\left\{ j2\pi B \frac{kT_s}{M} \left[\frac{a}{M} - \frac{1}{2} + k\frac{BT_s}{2M^2} - u\left(\frac{kT_s}{M} - \frac{M-a}{B} \right) \right] \right\} \\ &= \exp\left\{ j2\pi Bk \left[\frac{a}{M} - \frac{1}{2} + \frac{k}{2M} - u\left(\frac{k-M+a}{B} \right) \right] \right\} \\ &= \exp\left\{ j2\pi k \left[\frac{a}{M} - \frac{1}{2} + \frac{k}{2M} \right] \right\}, \qquad k = 0, 1, ..., M-1 \end{aligned} \tag{3.8}$$

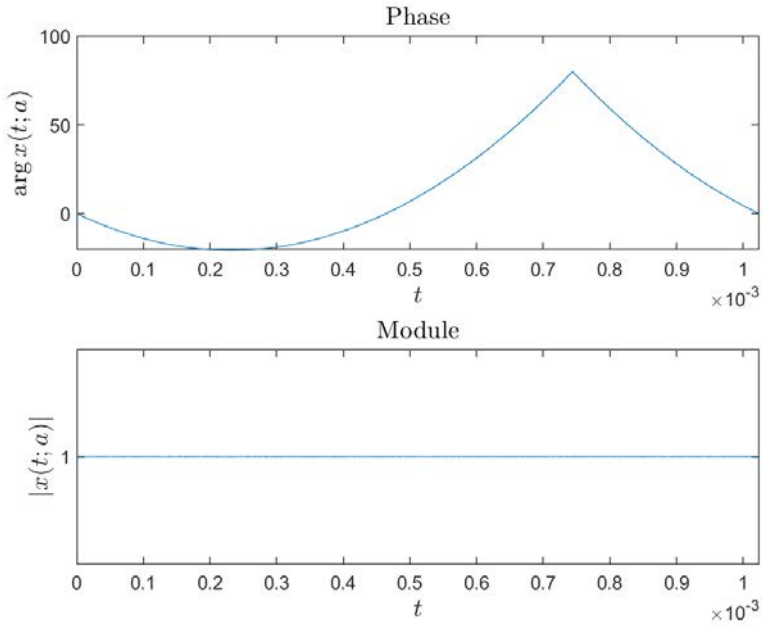

Figure 3.5: Plot of the phase and the modulus of a LoRa signal $x(t;a)$ with $a = 35, B = 125kHz$ and $SF = 7$.

where the last equality comes from the fact that $2\pi ku(\cdot)$ is always an integer multiple of 2π. The last observation let us neglect the modulus operation in the discrete time equation.

3.2 Properties

In this section we will analyse two properties that contradistinguish the LoRa signals and make them an even more appealing technology. The first property concerns the continuous version of the signal, while the second one regards the discrete equations of the LoRa modulation.

Property 1 (Continuous Phase)**.** *LoRa is a continuous phase modulation, i.e., the phase trajectory is continuous between any two consecutive symbols as well as during the transmission of any symbol.*

Proof. To prove the previous property we need to verify that the initial and the final phase of a generic symbol coincides.

So the initial phase is:

$$\Phi(0;a) = 0$$

while the phase at the end of the symbol is:

$$\begin{aligned}\Phi(T_s;a) &= 2\pi\left[\frac{a}{M}BT_s - \frac{1}{2}BT_s + \frac{1}{2M}B^2T_s^2 - BT_s u\left(T_s - \frac{M-a}{B}\right)\right] \\ &= 2\pi\left[a - \frac{M}{2} + \frac{M}{2} - Mu\left(\frac{M-M+a}{B}\right)\right] \\ &= 2\pi\left[a - Mu\left(\frac{a}{B}\right)\right] = 0\end{aligned}$$

The last equality is valid because a and M are always to integer values and then they can be simplified. Since $\Phi(0;a) = \Phi(T_s;a) = 0$ irrespectively of the value a, the property is proven. □

The continuity of the signal phase is of crucial importance to achieve the low power operation of LoRa devices. As a matter of fact it ensures that the power amplifiers of LoRa can be operated in satured mode without impairments in the transmitted signal.

The other property concerns the cross-correlation of the LoRa symbols in the discrete domain.

Property 2 (Symbol Orthogonality)**.** *The LoRa waveforms x(t;a) when sampled at time instants kT, with* $k \in \{0, 1, ..., M-1\}$ *form an orthogonal base.*

Proof. To prove the statement we compute the inner product between two generic LoRa symbols a_1 and a_2, with $a_1, a_2 \in \{0, 1, ..., M-1\}$ and $a_1 \neq a_2$:

$$\begin{aligned}&\sum_{k=0}^{M-1} x(kT;a_1)\cdot x^*(kT;a_2) \\ &= \sum_{k=0}^{M-1} e^{\jmath 2\pi k\left(\frac{a_1}{M} - \frac{1}{2} + \frac{k}{2M}\right)} \cdot e^{-\jmath 2\pi k\left(\frac{a_2}{M} - \frac{1}{2} + \frac{k}{2M}\right)} \\ &= \sum_{k=0}^{M-1} e^{\jmath 2\pi k\left(\frac{a_1}{M} - \frac{1}{2} + \frac{k}{2M} - \frac{a_2}{M} + \frac{1}{2} - \frac{k}{2M}\right)} \\ &= \sum_{k=0}^{M-1} e^{\jmath \frac{2\pi k}{M}(a_1 - a_2)}\end{aligned}$$

which can be interpreted as a geometric series and so

$$\begin{aligned}&\sum_{k=0}^{M-1}\left[e^{j\frac{2\pi}{M}(a_1-a_2)}\right]^k\\=&\frac{1-e^{j\frac{2\pi M}{M}(a_1-a_2)}}{1-e^{j\frac{2\pi}{M}(a_1-a_2)}}=0\end{aligned}$$

Therefore all the LoRa signals that are modulated with different symbols are orthogonal in the discrete time domain. □

The last property plays a crucial role to find the optimal receiver for the sampled waveform, which will be described in the next section, and it will be also fundamental for the derivation of the DOLoRa modulation in Chapter 5.

Finally in [17] it is proven a similar property for the continuous version of the waveforms, which can be considered orthogonal with a very good approximation also in the continuous time domain.

3.3 Demodulation

In this section we will focus on the receiver part of the LoRa system, where takes place the demodulation of the LoRa waveforms. Since the LoRa receiver, as for any other kind of system, samples the incoming signal before processing it, here we will use the discrete equations of the LoRa modulation (3.8).

At fist we will describe the structure of the optimum LoRa receiver, then we will introduce an efficient way to implement it, and finally we will analyse the characteristic *dechirping* process of the LoRa systems.

3.3.1 Optimum Receiver

Let's define $r(kT)$, $k \in \{0, 1, ..., M-1\}$ the received signal without the effect of noise. Now we can introduce $r_{AWGN}(kT) = r(kT)+n(kT)$, with $k \in \{0, 1, ..., M-1\}$, which is the actual received signal in the interval $\{0, T, ..., (M-1)T\}$, subject to an Additive White Gaussian Noise (AWGN) channel i.e, $n(kT)$ is a White Gaussian Noise with constant Power Spectral Density equal to $\frac{N_0}{2}$. The optimum non-coherent receiver (see [32]) for $r_{AWGN}(kT)$ is achieved in three steps:

1. Compute the cross correlation between the received signal and any possible waveform, and take the modulus square:

$$C(a) = \left| \sum_{k=0}^{M-1} r_{AWGN}(kT) \cdot e^{-\jmath 2\pi k\left(\frac{a}{M}-\frac{1}{2}+\frac{k}{2M}\right)} \right|^2 \quad \forall a \in \{0, 1, \ldots, M-1\} \tag{3.9}$$

2. Find the symbol a^* that maximizes the function $C(a)$ i.e., a^* is such that $C(a^*) \geq C(a), \forall a \in \{0, 1, \ldots, M-1\}$.
3. Decide that the transmitted symbol is a^*.

We have derived the optimum receiver in a very conservative manner, without paying attention on the actual implementation costs. In the next section we will see how it can be improved the demodulation process, by means of the *dechirping* technique.

3.3.2 Efficient Optimum Receiver

As we have already anticipated the optimum receiver can be further improved [16] by looking at (3.9) and rewriting it in a different way

$$C(a) = \left| \sum_{k=0}^{M-1} r_{AWGN}(kT) \cdot e^{-\jmath 2\pi k\left(\frac{k}{2M}-\frac{1}{2}\right)} \cdot e^{-\jmath 2\pi \frac{ak}{M}} \right|^2 \tag{3.10}$$

It should be clear that the previous computation is equivalent to the modulus square of the Discrete Fourier Transform (DFT) of the term $r_{AWGN}(kT)$ multiplied by $e^{-\jmath 2\pi k\left(\frac{k}{2M}-\frac{1}{2}\right)}$. So now we can modify the optimum receiver and get an *efficient* optimum receiver in only four steps:

1. Multiply $r_{AWGN}(kT)$ by $e^{-\jmath 2\pi \frac{k^2}{2M}+\jmath\pi k}$:

$$r_d(kT) = r_{AWGN}(kT) \cdot e^{-\jmath 2\pi \frac{k^2}{2M}+\jmath\pi k} \tag{3.11}$$

2. Apply the DFT or better the Fast Fourier Transform (FFT) to $r_d(kT)$ and obtain $R(a)$, that is a function of the symbols set.
3. Find the symbol a^* that maximize $\tilde{C}(a) = |R(a)|^2$ i.e., a^* is such that $\tilde{C}(a^*) \geq \tilde{C}(a)$, $\forall a \in \{0, 1, \ldots, M-1\}$.
4. Decide that the transmitted symbol is a^*.

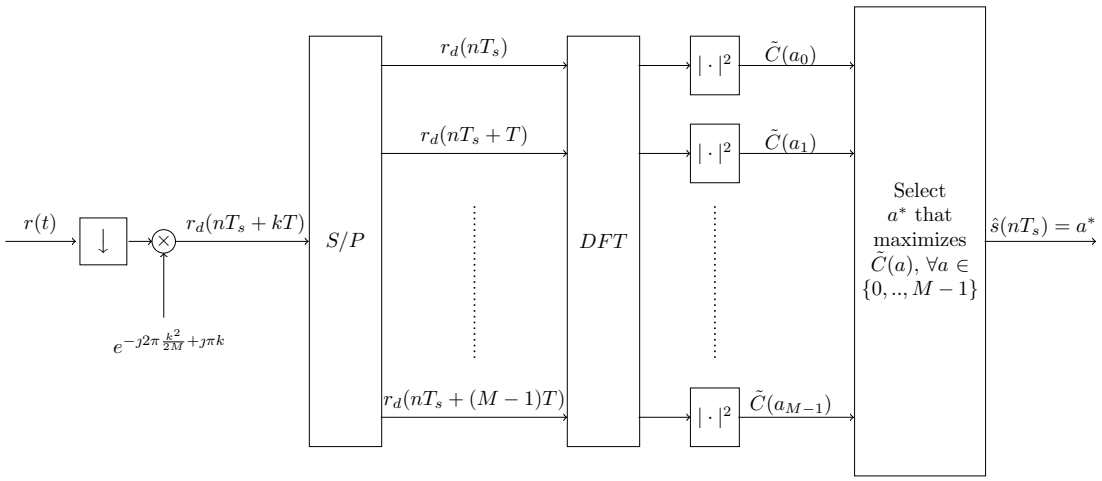

Figure 3.6: LoRa efficient optimum receiver. Noise is neglected.

This last receiver is optimal only under the assumption of AWGN, so at this point we need to demonstrate that after all the previous steps the noise $n(kT)$ remains white and gaussian.

Proof. The DFT is a linear filter and clearly it does not affect the gaussianity of the noise neither its variance. What we need to actually prove is the fact that $n_d = n(kT) \cdot e^{-\jmath 2\pi \frac{k^2}{2M} + \jmath\pi k}$ is white:

$$\begin{aligned}
&\mathbb{E}\left[n_d(kT) \cdot n_d^*(pT)\right] = \\
=&\mathbb{E}\left[n(kT)e^{-\jmath 2\pi \frac{k^2}{2M} + \jmath\pi k} \cdot n(pT)^* e^{+\jmath 2\pi \frac{p^2}{2M} - \jmath\pi p}\right] \\
=&e^{\jmath\pi(k-p)} \cdot e^{-\jmath \frac{2\pi}{2M}(k^2-p^2)} \mathbb{E}\left[(n(kT))\,(n(pT)^*)\right] \\
=&e^{\jmath\pi(k-p)} \cdot e^{-\jmath \frac{2\pi}{2M}(k^2-p^2)} \cdot N_0 \cdot \delta(p-k)
\end{aligned}$$

where, $\delta(p-k) = 1$ if $p = k$, otherwise it is zero. Then the noise remains white and gaussian and this concludes our prove. □

Finally in Figure 3.6 we can see a possible implementation of the efficient optimum receiver.

3.3.3 LoRa Dechirping

The LoRa demodulation is characterized by the *dechirping* operation, which is nothing more than a multiplication by the special term

$$e^{-\jmath 2\pi \frac{k^2}{2M} + \jmath \pi k} \tag{3.12}$$

Now we want to investigate what is going on behind the scene while we perform this multiplication.

Let's consider the time window $t \in [0, T_s[$, that corresponds to the transmission of a single LoRa symbol. To understand the effects of the dechirping, for ease of simplicity, we will consider that the baseband representation of the received signal $r'(kT)$ is the perfect downsampled copy of the baseband version $x(kT)$ of the original LoRa signal transmitted $s(t)$. In other words we are assuming to have and ideal channel (i.e, its impulse function is a delta function), that does not modify our transmitted signal. Moreover we are also not considering the noise. So from (3.8) we get

$$r'(kT) = x(kT) = e^{\jmath 2\pi k \left[\frac{a}{M} - \frac{1}{2} + \frac{k}{2M}\right]}, \quad k \in \{0, 1, \ldots, M-1\} \tag{3.13}$$

Note that $k \in \{0, 1, \ldots, M-1\}$, because of the previous assumption on the considered time interval.

The dechirping operation is then defined as

$$\begin{aligned} r'_d(kT) &= r'(kT) \cdot e^{-\jmath 2\pi \frac{k^2}{2M} + \jmath \pi k} \\ &= e^{\jmath 2\pi k \left[\frac{a}{M} - \frac{1}{2} + \frac{k}{2M}\right]} \cdot e^{-\jmath 2\pi \frac{k^2}{2M} + \jmath \pi k} \\ &= e^{\jmath 2\pi k \left[\frac{a}{M} - \frac{1}{2} + \frac{k}{2M} + \frac{1}{2} - \frac{k}{2M}\right]} \\ &= e^{\jmath 2\pi k \left[\frac{a}{M}\right]} \end{aligned}$$

which is a single impulse tone in the discrete domain, whose "frequency" a can be immediately find out with a Discrete Fourier Transform. This operation can be interpreted in the frequency domain as a process that collects all the original signal energy, spread over all the signal band, into a single frequency.

In Figure 3.7 is represented a LoRa signal modulated with the symbol $a = 35$

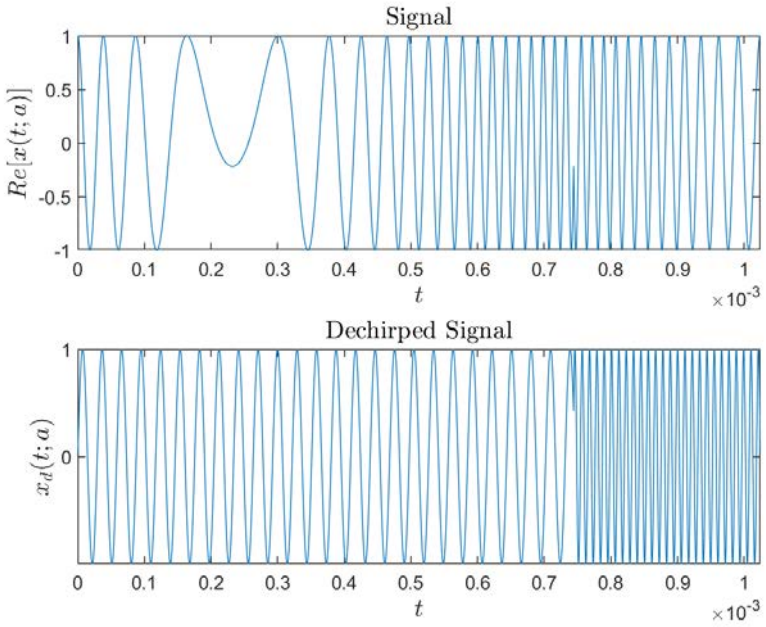

Figure 3.7: In the graph above is plotted the real part of the LoRa symbol $a = 35$ with $B = 125kHz$ and $SF = 7$. While in the graph below there is the dechirped version of the same signal.

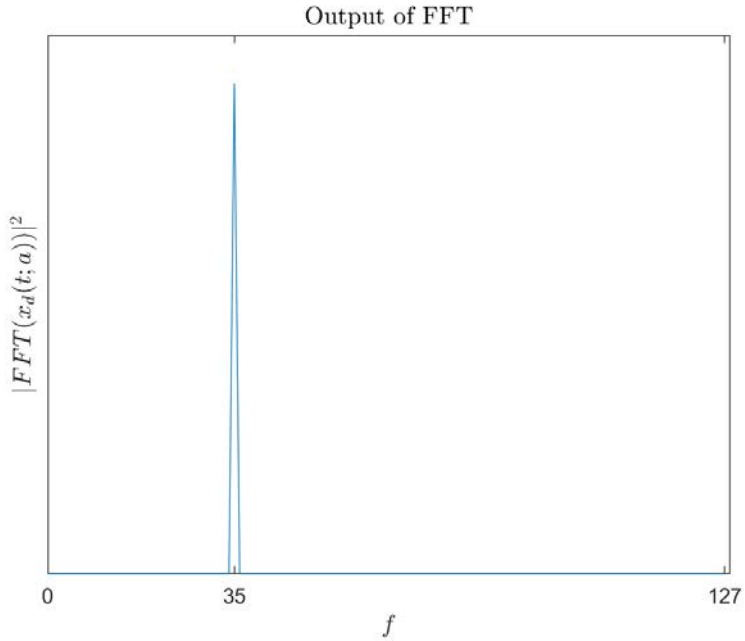

Figure 3.8: Output of the FFT applied on the dechirped version of a LoRa signal modulated with the symbol $a = 35$ with $B = 125kHz$ and $SF = 7$.

and the corresponding output from the dechirping operation, in the continuous time domain. It is interesting to notice that in the continuous time domain the dechirped signal is composed by two part with different frequencies, whose difference is exactly equal to B. This is why in the discrete domain we have found that the dechirped signal seems to contain only one tone impulse.

In conclusion in Figure 3.8 is shown the modulus square of the DFT of the previous signal, and as we expected, there is a peak in correspondence of the frequency $f = 35$. In fact the transmitted symbols was exactly $a = 35$.

4

Isolation between Spreading Factors

One of the hottest topics is the analysis of the LoRaWAN network capacity, that is investigated by means of simulations, such as in [7], or through analytical derivations as in [33, 34, 35].

In both the types of analysis the most fragile point is how the interference between LoRa signal with different Spreading Factors is threated. In fact in the LoRa literature there are several opinions on Spreading Factor pseudo-orthogonality and everything become even more confused and chaotic when we need to quantify the isolation between the sub-channels, induced by different Spreading Factors.

In [1] we find the first attempt to quantify this separation in terms of SINR (signal-to-interference-plus-noise ratio) difference between the signals under consideration. The main problem with these values is that they are provided without any reasoning or any explanation on how they are obtained. Moreover these threshold are quite different from the one obtained in a more recent paper [27], where the results are first computed through MATLAB simulations and then partially confirmed by USRP (Universal Software Radio Peripheral) experiments.

Even though the MATLAB's threshold are not perfectly matching the one obtained in practice, the two results can be considered a good approximation of the real case, at least as an estimation of the order of magnitude of sub-channels separation.

It is also important to say that the threshold in [27] are computed in term of

SIR (Signal-to-interference ratio) and not in SINR as in [1].

Now in this chapter we will describe a MATLAB simulator we have made to compute the co-channels rejection thresholds for different spreading factors, taking into account the work already done in [27].

4.1 Simulations Setup

The rejection thresholds between signals with different spreading factors will be calculated trough some simulations; the values will be expressed in terms of SIR.

For ease of simplicity from now on we will consider only two packets, since that the results can be easily generalized to the more common case of multiple packets. One packet will be considered as the *reference* packet, which is the packet that we desire to survive the interference, while the other one will be called *interfering* packet since we consider it as the packet that interferes with the first one.

The two packets interfere with each other when they start overlapping, but this overlap can be either partial or complete. Obviously the results from these two situations can be very different. So in our simulations, in order to have a common base to analyse and compare the results, we decided to take into consideration only the situations where the interfering packet is always completely overlapping with the reference packet. The target situations for the simulations are shown in Figure 4.1, where the red rectangle represent the region in which we are going to analyse the interference between the two packets. The packet above is the desired packet while the one below is the colliding packet. In the figure are represented the following situations: the collision of two packets with the same SF (Figure 4.1a) and the interference of two packets with different SF (Figure 4.1b and Figure 4.1c).

Given the length (in bytes) of the reference packet's payload as a parameter N_{bytes}, the number of bits in the packet is computed as

$$N_{bits_r} = \left\lceil \frac{8N_{bytes}}{(4N_{bs_r})} \right\rceil \cdot (4N_{bs_r}) \tag{4.1}$$

where N_{bs_r} corresponds to the number of bits contained in each symbol, which in our case corresponds to Spreading Factor of the reference packet, SF_r.
From this formula it is easy to compute the number of chirps inside every packet

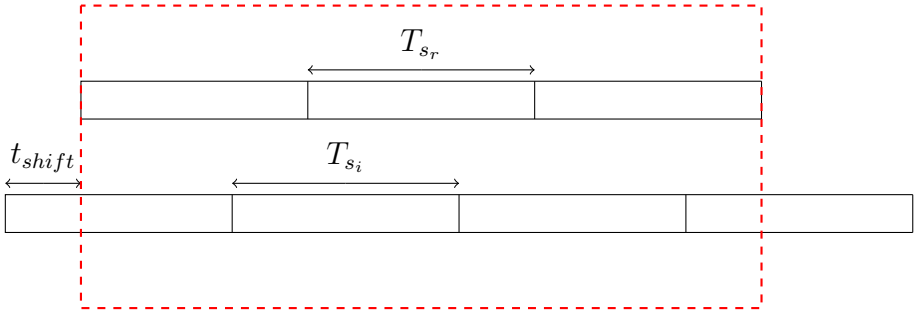

(a) The two packets have the same SF.

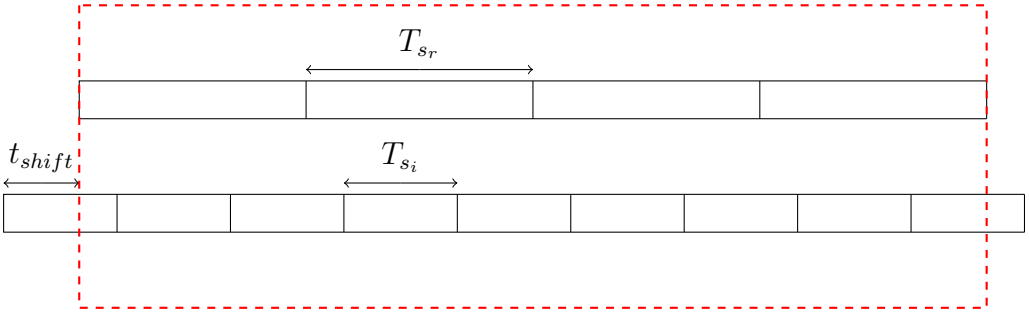

(b) The desired packet have an higher spreading factor than the colliding packet.

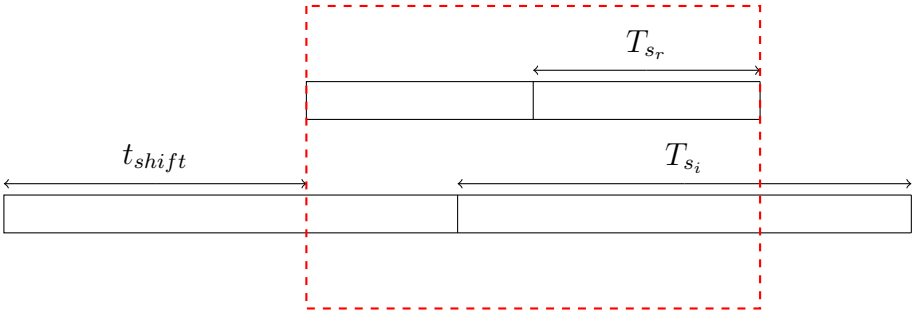

(c) The desired packet have a lower spreading factor than the colliding packet.

Figure 4.1: In each figure there are two colliding packets: the reference packet (above) and the interfering packet (below). In red is represented the window of our analysis.

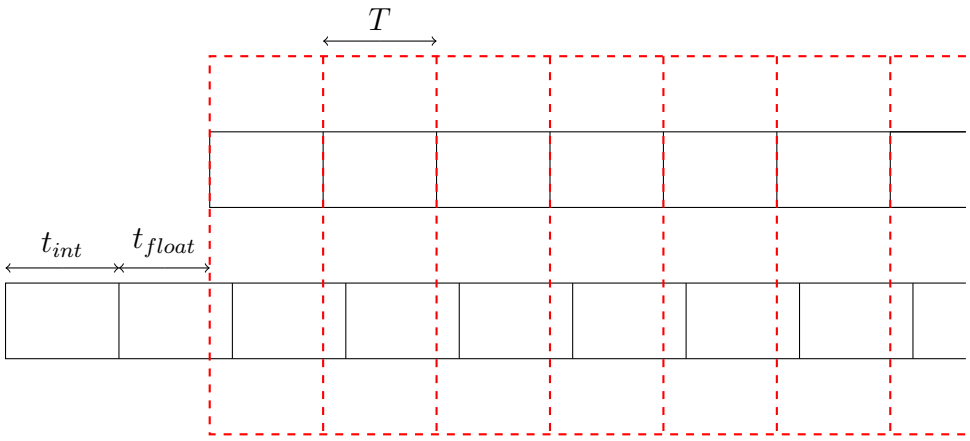

Figure 4.2: Alignment of two interfering packets. The packet above is the reference packet, which is synchronized with the receiver (represented in red). While the packet below is the interfering one and it is randomly shifted.

$$N_{chirp_r} = \left\lceil \frac{N_{bits}(CR+4)}{4N_{bs_r}} \right\rceil \tag{4.2}$$

where $4/(CR+4)$ with $CR \in \{0,1,2,3\}$ is the coding rate.
The time on air of the packet is

$$ToA = N_{chirp_r} \cdot M_r \tag{4.3}$$

All these results are used to obtain the complete overlap between the two packets, in fact the total number of chirp that the interfering packet should have is

$$N_{chirp_i} = \left\lceil \frac{ToA}{M_i} \right\rceil + 1 \tag{4.4}$$

where the $+1$ is added to compensate the effects due to the shift of the interfering packet with respect to the desired one.

To explain how the interfering packet is shifted we need to consider Figure 4.2 that represent the reference packet, the one above, and the interfering packet, the one below. Every square inside each packet corresponds to one chip, which last $T = 1/B$ seconds. The sampling time of the receiver is drawn in red, and as we can see from the image, it is perfectly synchronized with the sampling time of the reference packet. At this point come into place the shift of the interfering

packet, indeed from the figure it is clear that the receiver is sampling the signal asynchronously with respect to the sampling time (black vertical bars) of the interfering packet. In particular the packet is shifted randomly by

$$t_{shift} = t_{int} + t_{float} \tag{4.5}$$

where t_{int} is a shift of an integer number of sample, that is $t_{int} = n_{int}T$ with $n_{int} \in \{0, 1, 2, ..., M-1\}$ and this is the real reason why we have previously added one to the N_{chirp_i}.

The floating shift t_{float} is instead a fractional part of one chip period and is defined as

$$t_{float} = n_{float}\frac{T}{SR}, \qquad n \in \{0, 1, 2, ..., SR-1\} \tag{4.6}$$

where SR is a variable parameter.

Every time that we simulate two new interfering packets we generate t_{shift} by randomly drawing n_{int} and n_{float} from their respective set of values.

There is another parameter that we need to control, the power of the signal involved and in particular their ratio, or better their SIR

$$SIR = 10\log_{10}\frac{P_r}{P_i} = 10\log_{10}\frac{A_r^2}{A_i^2} \tag{4.7}$$

the tuning is done on the signals amplitude A_r and A_i.

More in details the two packets are built in such a way to have unitary power, then the refence packet is multiplied by $A_r = 1$, while the interfering packet is multiplied by A_i computed as follow

$$A_i = \frac{A_r}{10^{(\frac{SIR}{20})}} \tag{4.8}$$

To speed up the simulations the computation of the interfering signal shifted by t_{float} is done using the continuous time equation of the LoRa chirps in (3.6) sampled only on the time instants of our interest, which means at the sampling time of the receiver (the vertical dashed red lines in Figure 4.2).

4.2 Simulations Explained

Having described how to build the packets, we are ready to describe the real core of the simulator implemented in MATLAB, that is reported in Algorithm 4.1. First of all we need to choose the values of some parameters common to all the

Algorithm 4.1 MATLAB Simulation Structure.

Input: $B, CR, SR, L, SIR_{range}, SIR_{step}, BER_{target}, N_{err}$ and N_{iter}
Output: matrix SIR_{mat}

initialize empty SIR_{mat}
initialize SIR_{vec} by means of SIR_{range} and SIR_{step}
for all SF_r
    for all SF_i
        for all SIR in SIR_{vec}
            $n_{iter} \leftarrow 0$
            $n_{err} \leftarrow 0$
            create BER_{vec} to store all the BER for every SIR value
            while $n_{iter} < N_{iter}$ or $n_{err} < N_{err}$
                $p_r \leftarrow$ generate the signal of the reference packet
                $p_i \leftarrow$ generate the signal of the interfering packet
                randomly shift the interfering signal
                $p \leftarrow A_i \cdot p_i + A_r \cdot p_r$
                demodulate p
                update n_{err}
                $n_{iter} \leftarrow n_{iter} + 1$
            compute the BER for the actual SIR and store it in BER_{vec}
        use BER_{vec} to find the rejection threshold SIR_{th} associated to BER_{target}
        save SIR_{th} in the matrix SIR_{mat}
    return SIR_{mat}

simulations:

- B, the bandwidth of the signals.
- CR, parameter associated to the coding rate $\mathcal{C} = \frac{4}{4+CR}$.

- SR, the number of subsamples inside every sample of time $T = \frac{1}{B}$. We recall that it is used for the fractional shift of the colliding packet (4.6).
- L, the length of the reference packet expressed in bytes.
- SIR_{range}, the interval of SIR to test the rejection thresholds of the Spreading Factors. After every simulation the SIR is increased of SIR_{step} dB.
- BER_{target}, the target Bit Error Rate that determins the SIR rejection threshold.
- N_{err}, the minimum number of errors to be observed during simulations before changing the SIR value.
- N_{iter}, the minimum number of collisions to simulate before changing the SIR value.

The simulations are conducted in the following way. We build and initialize the output matrix SIR_{mat}, whose entries will be the rejection SIR threshold for every reference-interfering spreading factor combination (we will see an example of SIR_{mat} in the next section). We also create the vector SIR_{vec} by picking the SIR values from the interval SIR_{range} at steps of SIR_{step}. This vector will contain all the SIRs that we will use for our simulations.

Then for every possible situation, which means for every possible reference signal spreading factor and colliding signal spreading factor combination, we create an auxiliary vector BER_{vec} and then iterate over all the SIR inside SIR_{vec}. For each SIR value we simulate multiple times the collision of the two packets, whose content is randomly generated in every iteration, until we experience a minimum number of errors N_{err} and we reach a minimum number of simulated packet collisions N_{iter}. The interfering packet is randomly shifted every time with a different t_{shift} according to (4.5). After this block of simulations we compute the corresponding BER for the specific SIR value, and we store it in BER_{vec}. When we have collected all the bit error rate associated to each SIR in SIR_{range} we can compute the rejection threshold corresponding to BER_{target}, which will be stored in the matrix SIR_{mat}.

Finally we remark that in every iteration of the inner while loop of Algorithm 4.1, all the bits inside the reference packet are encoded with a code rate $\mathcal{C} = \frac{4}{4+CR}$ and it is also used a Gray mapping. The simulations parameters are summarized in Table 4.1.

Parameter	Value
B [kHz]	125
$\mathcal{C}$	4/5
L [bytes]	20
SIR_{range} [dB]	[-30, 10]
SIR_{step} [dB]	1
BER_{target}	0.01
SR	100
N_{iter}	$4 \cdot 10^3$
N_{err}	100

Table 4.1: Simulation Parameters.

SF_r \ SF_i	7	8	9	10	11	12
7	0	-10	-12	-13	-13	-14
8	-13	0	-13	-14	-16	-16
9	-16	-15	0	-16	-17	-18
10	-18	-19	-18	0	-19	-20
11	-21	-21	-21	-21	0	-21
12	-23	-24	-24	-24	-24	0

Table 4.2: SIR rejection thresholds [dB] computed in MATLAB for the standard LoRa modulation

4.3 Results of the simulations

The results of the MATLAB simulations for the standard LoRa modulation are summarize in Table 4.2. The meaning of these values is quite immediate if we consider the formula of SIR:

$$SIR = \frac{P_r}{P_i} \tag{4.9}$$

where P_r is the power of the reference packet and P_i is the power of the interfering packet. In the logarithmic domain the expression becomes:

$$SIR_{dB} = 10\log_{10}(P_r) - 10\log_{10}(P_i) \tag{4.10}$$

Therefore the thresholds are nothing else than the minimum value that SIR_{dB} should have in order to let the reference packet survive to the interference caused by the colliding packet.

From now on in this section we will interpret the Table 4.2 as a matrix. Each entry of the matrix, $SIR_{q,j}$, is identified by its row index q, and its column index j, that corresponds to the employed spreading factors and so $q, j \in \{7, 8, \ldots, 12\}$. For example if the desired packet has $SF = 8$ and the interfering one has $SF = 10$, the receiver will successfully demodulate and decode the reference packet if and only if $10\log_{10}(P_r) - 10\log_{10}(P_i) > SIR_{8,10} = -14$ dB.

As anticipate these results coincide to the one in [27].

It is interesting to notice the beneficial consequences of the channel capture effect, that in the case of two colliding packets with the same spreading factor, allows the decoding of one packet if it has an higher power than the other one (the rejection factor is always zero for all SF). In general we can notice that the packets with an high SF (e.g. 11 or 12) are more resilient to interference than the one with a low SF (e.g. 7 or 8). However an higher spreading factor means a longer time on air and as a consequence an higher probability of packet collision.

In Figure 4.3 we can see the behaviour of the BER of the two colliding packet, when the SIR is varying inside the interval SIR_{range}.

Usually when we perform some simulations it is also important to compute the confidence interval associated to the results. In our simulations we have carried out n independent bit transmission for every spreading factor combination and we were interested in a binary outcome (success or failure). This situation can be mathematically described as a sequence of n independent Bernoulli random variables $X_1, X_2, \ldots, X_n$ with success probability equal to $p = BER$. A natural estimator of p is $\frac{1}{n}\sum_{k=1}^{n} X_i$, which coincide to the mean of the outcomes [36].

In [36] it is also stated a theorem to compute the confidence interval for this defined model. In particular it says that if we have observed z successes out of n independent experiments, a confidence interval at level γ for the success probability p is $[L(z), U(z)]$ with

$$\begin{cases} L(0) = 0 \\ L(z) = \Phi_{N,z-1}\left(\frac{1+\gamma}{2}\right), \quad z = 1, \ldots, n \\ U(z) = 1 - L(n-z) \end{cases} \tag{4.11}$$

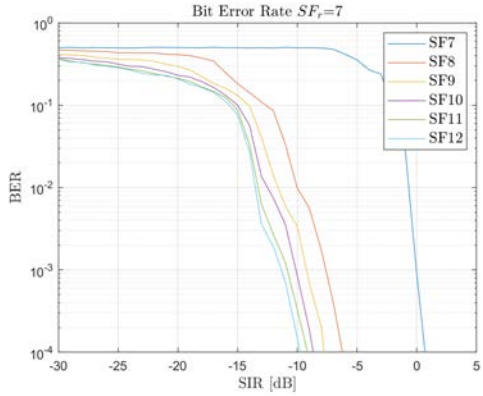

(a) The reference packet has SF=7.

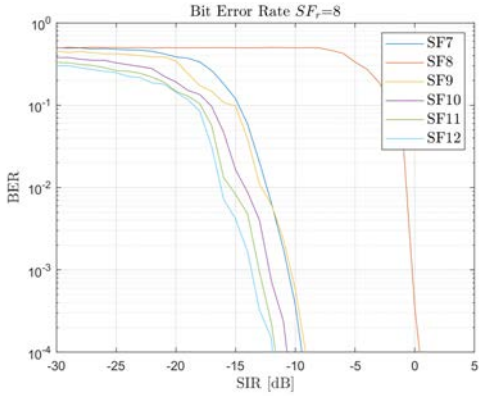

(b) The reference packet has SF=8.

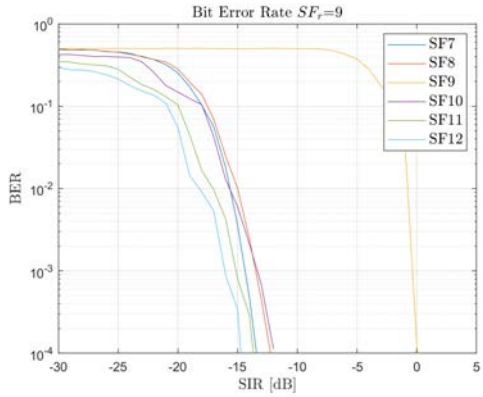

(c) The reference packet has SF=9.

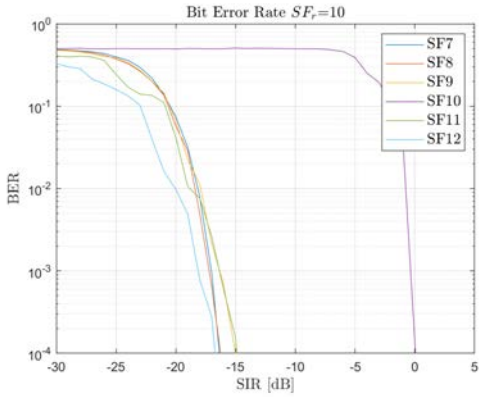

(d) The reference packet has SF=10.

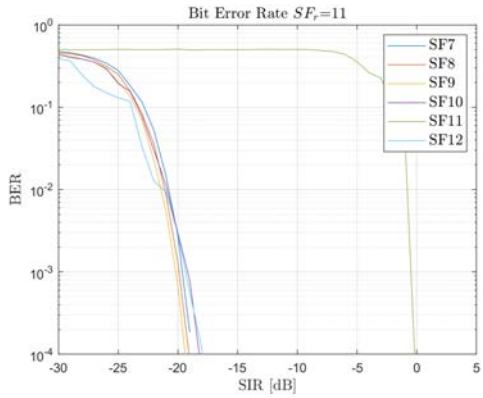

(e) The reference packet has SF=11.

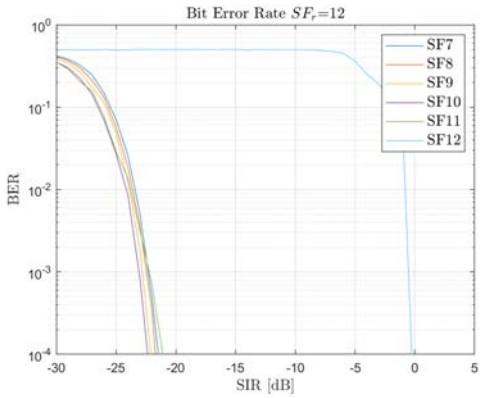

(f) The reference packet has SF=12.

Figure 4.3: Behaviour of the BER of two interfering packets with respect to their SIR.

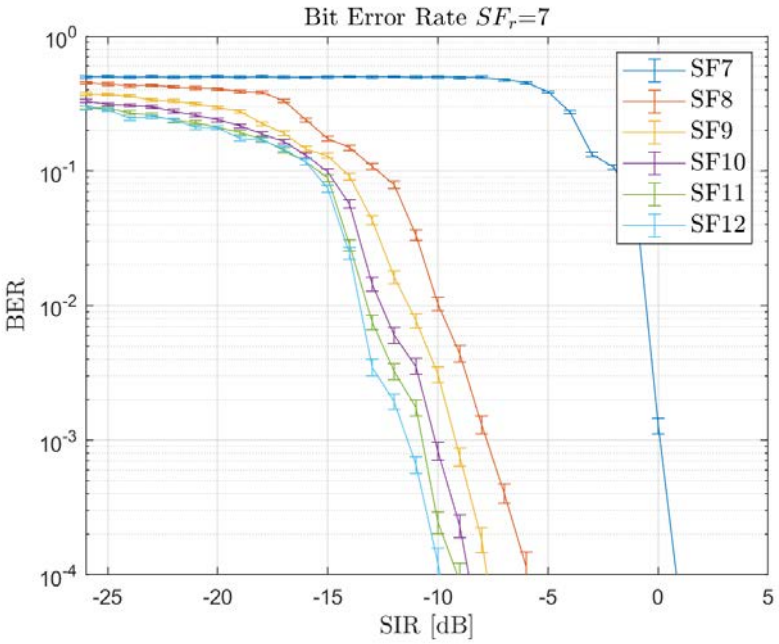

Figure 4.4: BER behaviour with vertical error bars of two interfering packets. The reference packet has SF=7.

where $\Phi_{n,z}(\alpha)$ is defined for $n = 2, 3, \ldots, z \in \{0, 1, 2, \ldots, n\}$ and $\alpha \in (0, 1)$ by

$$\begin{cases} \Phi_{n,z}(\alpha) = \frac{n_1 f}{n_2 + n_1 f} \\ n_1 = 2(z+1) \\ n_2 = 2(n-z) \\ 1 - \alpha = F_{n_1,n_2}(f) \end{cases} \tag{4.12}$$

where $F_{n_1,n_2}(\cdot)$ is the CDF of the Fisher distribution with n_1, n_2 degrees of freedom. While if we observe $z = 0$ successes the confidence interval for p is $[0; p_0(n)]$ with

$$p_0(n) = 1 - \left(\frac{1-\gamma}{2}\right)^{\frac{1}{n}} \tag{4.13}$$

By means of this tool we are able to compute the interval of confidence for all the BER values that we have already computed. These uncertainties, calculated with $\gamma = 0.98$, are all plotted as vertical bars in the graphs of Figure 4.4.

4.4 Generalization to multiple colliding packets

In real situations it is common to observe multiple colliding packet and it is very rare that they are all entirely overlapping. So in this section we will se how to adapt the SIR thresholds that we have computed to this more general case.

At first remark that, in presence of multiple interfering packets, the margins on the SIR must be met by all the colliding packets, summing up the received power values for each SF. Therefore we can generalize the definition of SIR in (4.9) as

$$SIR = \frac{P_r}{\sum_{l=1}^{N_{int}} P_{i,l}} \tag{4.14}$$

where P_r is the received power of the reference packet, N_{int} is the number of interfering packets, and $P_{i,l}$ is the power of the l-th colliding packet.

Now let's consider that our desired packet has $SF = q$, which we recall it also corresponds to the q-th row of the SIR matrix, and the set of all the interfering packets $\mathcal{I}$. The set $\mathcal{I}$ can be expressed as the disjoint union of six different other sets, each one collecting the devices with a specific spreading factor

$$\mathcal{I} = \mathcal{I}_7 + \mathcal{I}_8 + \ldots + \mathcal{I}_{12} \tag{4.15}$$

Therefore the packet will be successfully decoded by the receiver if

$$SIR_{dB} = 10 \log_{10} \left(\frac{P_r}{\sum_{l \in \mathcal{I}_j} P_{i,l}} \right) > SIR_{q,j}, \quad \forall j \in \{7, 8, \ldots, 12\} \tag{4.16}$$

Finally we need to find out a way to extend the threshold values, computed in the very specific case of two completely overlapping packets, to the more realistic situation of partially overlapping packets. The solution that we will adopt is the same described in [7], where is performed an operation of energy *equalization*. To explain the procedure we will consider Figure 4.5, where there are two colliding packets: one is received at time $t = 0$ with $SF_r = x$ and duration T_x, while the other is received at time t_1 with $SF_i = y$ and duration T_y. The energy of the packet x can be computed as $E_x = P_{r,x} \cdot T_x$ and the interfering energy is

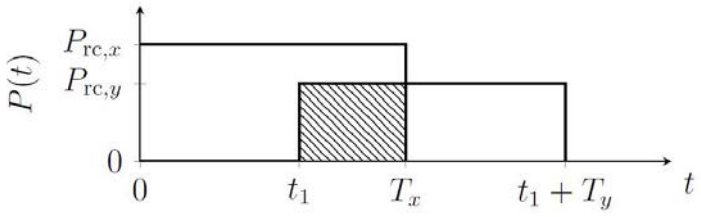

Figure 4.5: Power *equalization* of colliding packets. The highlighted energy is spread on the duration of the packet [7].

$E_i = P_{i,y} \cdot (T_x - t_1)$. At this point the *equalized* interfering power is:

$$P_i = \frac{E_i}{T_x} = \frac{P_{i,y}(T_x - t_1)}{T_x} \tag{4.17}$$

In other word, every time that we have some partially interfering packets, we take the interfering energy between the desired packet and all the other packets, and we can imaging to distribute it over the entire packet. In that way we are able to compute the SIR and evaluate its chances to survive by means of (4.16).

As we can read in [7] this assumption can be justified by the fact that in the underlying physical layer of the LoRa protocol is used an interleaver, whose aim is to distribute the interference along the entire signal, even though in the real channel we can experience a bursty interference that affects only a few number of symbols.

5

LoRaWAN Improvements

In this section two new innovative modulations are proposed to improve the performances of the LoRa systems at the LoRaWAN network level. The first one, called *DOLoRa* (Dual Orthogonal LoRa) modulation, aims at increasing the link level bitrate at the expense of a 3 dB penalty in SNR. The main idea behind it is of sending two symbols per LoRa chirp instead of only one per chirp. The second modulation, called *DLoRa* (Decreasing LoRa), is similar to the conventional LoRa modulation and it is compatible with it in terms of bandwidth and numerology. DLoRa departs from the standard Lora modulation as it is using a decreasing instantaneous frequency in the chirps, instead of an increasing one as for the conventional LoRa. The goal of this new modulation is to increase the number of the pseudo-orthogonal channels of LoRa, and as a consequence increase the capacity of the LoRaWAN networks.

The two improvements are provided through a cross-layer design framework, in fact they both act at the physical layer and despite they may be penalizing in this level, the final overall performances of the network level are increased. In particular this is valid for some special real-case scenarios.

In this Chapter at first we will give a brief introduction on the discrete event network simulator NS3 [20] and on the LoRaWAN module developed in [37]. Then we will discuss the two new modulations through an analytical approach, and finally we will analyse the two innovative DOLoRa and DLoRa schemes by

means of NS3 and SEM (Simulation Execution Manager) [38].

5.1 The simulator NS3

NS3 is a discrete-event network simulator for Internet Systems, targeted primarily for research and educational use. It is a free software publicly available for development and research use [20]. The simulator is composed by modules, each one implementing a different technology, e.g. there are modules for LTE, WiFi, Bluetooth and many other standards.

For our simulations we are interested in a recently developed module `lorawan`, that is able to simulate the LoRaWAN networks. This module collects all the necessary classes that work together to describe the behaviour of LoRa EDs and GWs from the Physical to the Application layer. However for our purposes we will limit the use of the module only to the PHY layer, in fact we will analyse the probability of successfully receiving a PHY packet at the gateway. All the LoRaWAN network part related to the NS will be neglected.

The propagation loss model adopted for the signal propagation in NS3 for our simulation is described by the following equation

$$P_{RX} = P_{TX} - L_0 - 10n \log_{10}\left(\frac{d}{d_0}\right) \tag{5.1}$$

where L_0 is the reference path loss of the model at the reference distance d_0, n is the path loss exponent, P_{TX} is the signal of the transmitted packet, and finally P_{RX} is the received power. Even though it is a simplified model it allow us to capture the general trend of the signal propagation while keeping the computational complexity of the simulations as low as possible. This model is used to calculate the received power of every packet and check if it is above the sensitivity of the GW S_{gw} or the ED S_{ed}, if the receiver are respectively the GW or the ED. The sensitivity of the devices is different for every spreading factor and it is summarized in Table 5.1.

Another important aspect that we need to explore is the techniques that are used inside the simulator to assign the spreading factors to the nodes. In particular we will exploit the standard method to assign the spreading factors plus other two modified version of it in order to take into account also the two new

SF	S_{gw} [dBm]	S_{ed} [dBm]
7	-130.0	-124
8	-132.5	-127
9	-135.0	-130
10	-137.5	-133
11	-140.0	-135
12	-142.5	-137

Table 5.1: Sensitivity of Gateways and End Devices at different Spreading Factors [9].

SF	Distance Range [m] from GW
7	1 - 2920
8	2920 - 3509
9	3509 - 4217
10	4217 - 5067
11	5067 - 5728
12	5728 - 6474

Table 5.2: Distances that delimits the ring region of each spreading factor.

modulation. For all our simulation the transmitting power of all the devices will be set to the maximum allowed ($P_{TX} = 14$ dBm) because the `lorawan` module is still lacking of an ADR algorithm.

As anticipated in Chapter 3 the spreading factors are given to nodes in such a way to let them transmit at the highest possible bitrate, while guaranteeing a robust communication link between the ED and the GW [39]. In other words every device will get the lowest spreading factors, which ensures that the received power of the packets from the GW will be higher than the ED sensitivity for the specific spreading factor.

Since our propagation model is deterministic and the received power depends only from the distance between the ED and the GW, by inverting (5.1), we can compute the limit radiuses that delimits the ring regions around the GW, where all node have the same SF. The limit distances will allow us to define for every spreading a ring shape area, that we will call *sf-regions*. These areas, whose limit distances are reported in Table 5.2, will be used to assign the SF to the EDs.

Parameter	Value
P_{TX}	14 dBm
L_0	7.7 dB
d_0	1 m
n	3.76

Table 5.3: Parameters for the simulations in NS3.

Before explaining the other two strategies we anticipate that, for almost every canonical spreading factor, the two new modulations provide an equivalent new spreading factor version, whose signals behaves in the same manner as the one built with the corresponding canonical spreading factor (we will better investigate this fact in the next sections). In particular, if we consider the previous relation between the node position and the SF, for every ring region the canonical and the new version of every SF* are available. So the first technique to decide the nodes spreading factors, when we have both the standard LoRa modulation and one of the new modulations, is to give to every node the standard or the new version of the SF randomly. The second strategy is to place a sensitivity threshold inside each SF-region in such a way to assign the canonical SF to the EDs below that threshold, and the new SF to the one above the threshold, or vice versa. We will call *random approach* the first method, and *sensitivity approach* the second one.

Finally all our simulations will be run with the parameter values in Table 5.3 and in a scenario, where the spreading factor distribution is equal to the real case situation reported in Table 5.4, taken from [10]. It is a very peculiar situation in which the vast majority of the devices have $SF = 7$ or $SF = 8$, and all the other spreading factors are almost unemployed. This scenario is modeled inside the NS3 simulator by deploying the nodes according to the sf-regions of Table 5.2.

5.2 DOLoRa (Dual Orthogonal LoRa)

The Dual Orthogonal Lora modulation, which is a new modulation scheme compatible with the standard LoRa modulation, aims at improving the LoRaWAN

*We remark that in this thesis will never use both DLoRa and DOLoRa at the same time.

SF	Percentage of EDs
7	76.51%
8	9.49%
9	5.20%
10	2.91%
11	1.25%
12	4.64%

Table 5.4: Distribution of Spreading factors in a LoRaWAN real life water metering application [10].

network level performances by providing additional levels of freedom to the Spreading Factors assignment. In this section the DOLoRa will be described analytically and then, we will analyse the improvement that it can bring in the network capacity.

5.2.1 Description of the modulation

As anticipated, the main idea behind this modulation is transmitting two symbols per LoRa chirp instead of only one. This can be done thanks to Property 2 of Chapter 3, which states that the waveforms (3.8) for different values of a are orthogonal in the discrete domain, and orthogonal with a very good approximation also in the continuous time domain [17].

Now let p and d two integer numbers ranging from 0 to $\frac{M}{2} - 1$. The integer p carries $SF - 1$ bits, and, in the same way, the integer d carries $SF - 1$ bits. So the two integers together carry a total of $2SF - 2$ bits. As a matter of fact it is convenient to introduce the binary notation of the two integers $\mathbf{p}^b$ and $\mathbf{d}^b$:

$$\mathbf{p}^b = [p_0^b, p_1^b, \ldots, p_{SF-2}^b] \tag{5.2}$$

$$\mathbf{d}^b = [d_0^b, d_1^b, \ldots, d_{SF-2}^b] \tag{5.3}$$

being $p_i^b, d_i^b \in \{0,1\}$, with $i = \{0,1,\ldots,SF-2\}$, so that:

$$p = \sum_{i=0}^{SF-12} p_i^b 2^i \tag{5.4}$$

$$d = \sum_{i=0}^{SF-12} d_i^b 2^i \tag{5.5}$$

The two numbers p and d can be considered as two LoRa symbols and then we can define the new signal $y(kT;p,d)$ in the interval time $[0,T_s[$ as

$$\begin{aligned} y(kT;p,d) = &\frac{1}{\sqrt{2}} \exp\left\{ j2\pi k \left[\frac{2p}{M} - \frac{1}{2} + \frac{k}{2M} \right] \right\} \\ &+ \frac{1}{\sqrt{2}} \exp\left\{ j2\pi k \left[\frac{2d+1}{M} - \frac{1}{2} + \frac{k}{2M} \right] \right\}, \qquad k = 0,1,\ldots,M-1 \end{aligned} \tag{5.6}$$

We will refer to this signal as a dual orthogonally modulated LoRa signal with Spreading Factor SF.

We remark that $y(kT;p,d)$ was created in such a way to have the same energy as the original signal $x(kT;a)$. The demodulation process to recover the symbols p and d, is performed in the usual way, with the difference that we will get a vector $\tilde{\mathbf{y}}$ whose k-th component is

$$\begin{aligned} \tilde{y}_k &= y(kT;p,d) \cdot e^{-j\frac{2\pi k^2}{2M} + j\pi k} \\ &= e^{j\frac{2\pi}{M}k\cdot 2p} + e^{j\frac{2\pi}{M}k\cdot(2d+1)}, \quad k = 0,1,\ldots,M-1 \end{aligned} \tag{5.7}$$

and then through the DFT $\mathbf{Y} = DFT(\tilde{\mathbf{y}})$ we can recover p' by tacking the maximum of the square modulus over the even indexes of $\mathbf{Y}$, and d' by tacking the maximum of the square modulus over the even indexes of $\mathbf{Y}$:

$$\begin{aligned} p' &= \underset{m=0,2,\ldots,M-2}{\arg\max} |\mathbf{Y}_m|^2 \\ d' &= \underset{m=1,3,\ldots,M-1}{\arg\max} |\mathbf{Y}_m|^2 \end{aligned} \tag{5.8}$$

which are related to p and d by means of the following equations

$$\begin{aligned} p &= \frac{p'}{2} \\ d &= \frac{d'-1}{2} \end{aligned} \tag{5.9}$$

In a totally equivalent manner the symbols p and d can be transmitted one in the first half of the samples and the other in the other half. The results will be the same in both the cases. The only difference stands on the complexity of the receiver detector implementation.

If we compare the DOLoRa modulation with the standard LoRa modulation, we can find out that:

- having the same SF the energy per bit $E_b^{dual}(SF)$ in the Dual Orthogonal LoRa modulation is reduced by a factor $\frac{SF}{2(SF-1)}$ which, for example considering $SF = 8$, is $\frac{8}{14}$ i.e. 2.43 dB.
- with the same ToA in the standard LoRa modulation we reduce the SF, the energy per bit $E_b^{std}(SF)$ is once again reduced by a factor $\frac{SF}{2(SF-1)}$. For example if we have one standard LoRa symbol with $SF = 8$ carrying 8 bits and two consecutive standard LoRa symbols with $SF = 7$ carrying 7 bits each, the penalty in energy per bit is $\frac{8}{14}$, i.e. 2.43 dB.

So resorting to DOLoRa modulation is then equivalent, from the Energy per bit and the duration of the transmission, to the standard LoRa modulation. Even though it seems that DOLoRa is not introducing any improvement to the LoRa systems, we will see that the advantages of this new modulation will be evident at the network layer.

In Figure 5.1 we can see the performances of DOLoRa and LoRa modulation. In particular it is interesting to notice that the DOLoRa modulation with spreading factor $k = 8, 9, 10, 11, 12$ has the same performances of the standard LoRa modulation with spreading factor $k - 1$. This can be easily justified by the fact that every DOLoRa signal carries two symbols with half the power (3 dB) of a regular symbol for the LoRa standard modulation. Moreover in the standard Lora modulation a symbol with $SF = k$, $k = 8, 9, 10, 11, 12$ uses twice (3 dB) the energy of a symbol with $SF = k - 1$.

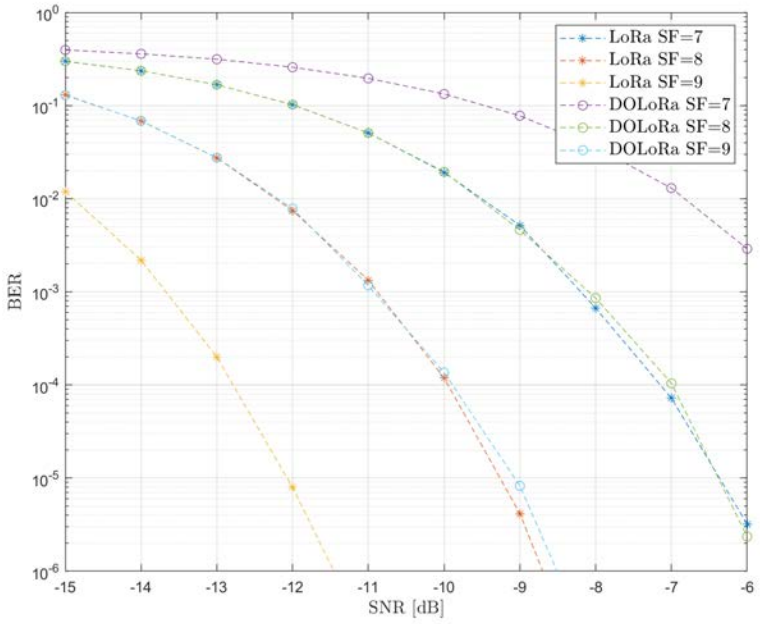

Figure 5.1: Performance of the standard and the Dual Orthogonal LoRa modulation.

In the LoRaWAN network the EDs spreading factors are decided by the ADR algorithm, which gives to nodes the minimum spreading factor while ensuring a sufficiently reliable link. If the operators need to improve the LoRaWAN network capacity, the easiest way to do that is by introducing new gateways in the area through the so called process of "network densification". Then, since the distance between the GWSs and the EDs will decrease, it will be more probable that the EDs will use in vast majority low SF (i.e. $SF = 7, 8, 9$) with the tendency to have most of the devices working with $SF = 7$.

In Chapter 4 we have found that the spreading factor can induce some pseudo-orthogonal channel, which can be considered orthogonal with sufficient approximation when evaluating the network performances, i.e. we can neglect the collisions between different SFs. For this reason in the extreme (but realistic) case of networks where all the EDs are employing $SF = 7$, the other *logical channels* provided by the other SFs are not used. Then the overall throughput of the network will strongly decrease due to the fact that the vast majority of LoRaWAN networks use the ALOHA channel access technique, which will led to a lot of collisions inside the virtual channel with $SF = 7$.

SF_{OS_r} \ SF_{OS_i}	7_1	8_1	9_1	10_1	11_1	12_1	8_2	9_2	10_2	11_2	12_2
7_1	0	-10	-12	-13	-13	-14	-10	-11	-11	-12	-12
8_1	-13	0	-13	-14	-16	-16	-3	-12	-14	-14	-15
9_1	-16	-15	0	-16	-17	-18	-15	-3	-15	-16	-17
10_1	-18	-19	-18	0	-19	-20	-18	-18	-3	-18	-19
11_1	-21	-21	-21	-21	0	-21	-21	-21	-21	-3	-21
12_1	-23	-24	-24	-24	-24	0	-23	-24	-24	-24	-3
8_2	-10	3	-10	-11	-13	-13	0	-10	-11	-11	-12
9_2	-13	-12	3	-13	-14	-15	-12	0	-13	-14	-14
10_2	-15	-16	-15	3	-16	-17	-15	-15	0	-15	-17
11_2	-18	-18	-19	-18	3	-17	-18	-18	-18	0	-18
12_2	-21	-21	-21	-21	-21	3	-21	-21	-21	-21	0

Table 5.5: Co-channel rejection threshold for DOLoRa and LoRa modulation combined together. The subscript on the SF indicates the number of orthogonal symbols OS, brought by every chirp.

In this situation come into place DOLoRa, which will allow us to use also the other SFs and in particular take advantage of their pseudo-orthogonality, without losing anything in terms of EDs' transmission bitrate. In fact transmitting two symbols with $SF = k$, $k = 7, 8, \ldots, 11$, or sending one DOLoRa symbol with $SF = k + 1$, takes the same amount of time and energy. However, as we anticipated in the previous section, we will also need to modify the ADR mechanism, which, every time the SNR is such that both the standard and the DOLoRa version of the SF can be used, will choose one of the two spreading factor by means of a threshold on the node sensitivity (*sensitivity approach*) or in a pure random way (*random approach*). In general with DOLoRa we will be able to better employ all the available SFs and in particular to better exploit their pseudo-orthogonality.

5.2.2 Simulations

First of all we need to generate the rejection thresholds for the DOLoRa modulation combined with the standard LoRa modulation, which are reported in Table 5.5. We remark that the subscript OS of each spreading factor SF indicates the number of orthogonal symbols brought by every chirp, which means that $OS = 1$ indicate the standard LoRa modulation while $OS = 2$ indicates the DOLoRa modulation. It is interesting to observe that the DOLoRa version of every

spreading factors introduces a penalty of 3 dB in the rejection thresholds, which is in perfect accordance with our previous argumentation.

To prove the advantages of the DOLoRa modulation we carried out some simulations in *ns3* by means of the module `lorawan`, which was modified according to specifications of the new modulation. From now on in this section, it is important to make the distinction between symbol period T_s and chirp period $T_{chirp} = M \cdot T$, because in the Dual Orthogonal LoRa modulation we send $OS = 2$ symbols per chirp, which leads us to say that every symbol is transmitted in $T_s = \frac{T_{chirp}}{OS}$ instead of T_{chirp}, even though this last claim is not exactly true. So the change introduced by the new modulation affects the ToA of the packets (2.5), where, while $t_{preamble}$ will remain the same for both the standard and the DOLoRa modulation, $t_{payload}$ should be modified as follows:

$$t_{payload} = \left\lceil \frac{n_{payload}}{OS} \right\rceil \cdot T_{chirp} \tag{5.10}$$

Also the computation of $n_{payload}$ will be different:

$$n_{payload} = 8 + \max\left(\left\lceil \frac{8PL - 4(SF - \log_2(OS)) + 28 + 16CRC + 20H}{4(SF - \log_2(OS) - 2DE)} \right\rceil (CR + 4), 0 \right) \tag{5.11}$$

Now we are going to investigate the performances of the new modulation in a real case scenario, which was depicted in Section 5.1. Our target is to analyse the advantages carried by DOLoRa in terms of probability to successfully transmit a PHY LoRa packet. This will be done by running multiple simulations in scenarios with an increasing number of EDs inside the LoRaWAN network. In Figures 5.2 we can see an example of network topology used for the simulations.

To achieve our goal we performed two campaign of simulations, whose results are shown in Figure 5.3. In the first campaign we distributed the SF between the EDs through the *random approach* (Figure 5.3a), while in the second we adopted the *sensitivity approach* (Figure 5.3b). The results are quite different. In fact the random approach performs worse than the sensitivity approach, which assigns the new DOLoRa spreading factors to the EDs with an higher reception power. This happens because the DOLoRa version of every spreading factor has a penalty of 3 dB in the rejection SIR threshold against the standard version, i.e. a packet with $SF_{OS} = k_2$, $k = 8, 9, 10, 11, 12$ colliding with a packet with $SF_{OS} = k_1$ will survive

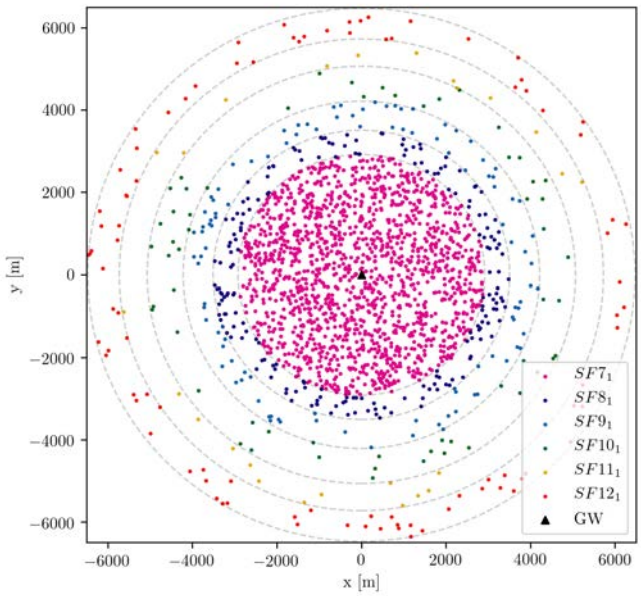

(a) The network topology with only the standard modulation.

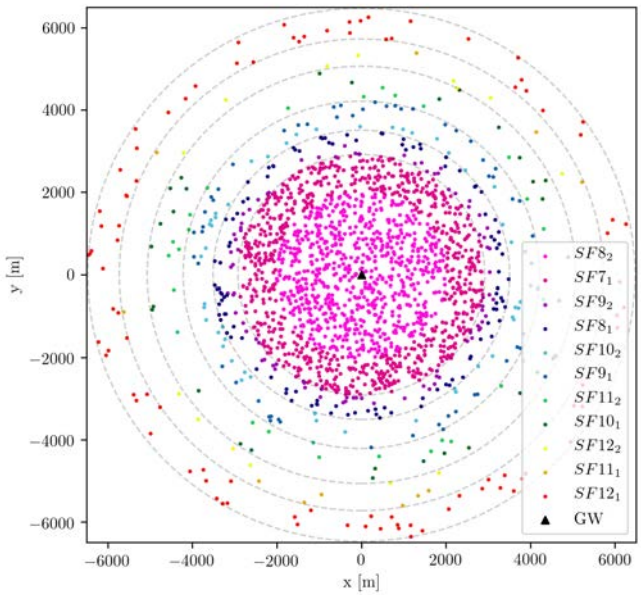

(b) The network topology with the standard and the dual orthogonal LoRa modulation.

Figure 5.2: Topologies of the network under analysis. In both the images there are 2000 devices. The dashed circles delimit the different sf-regions.

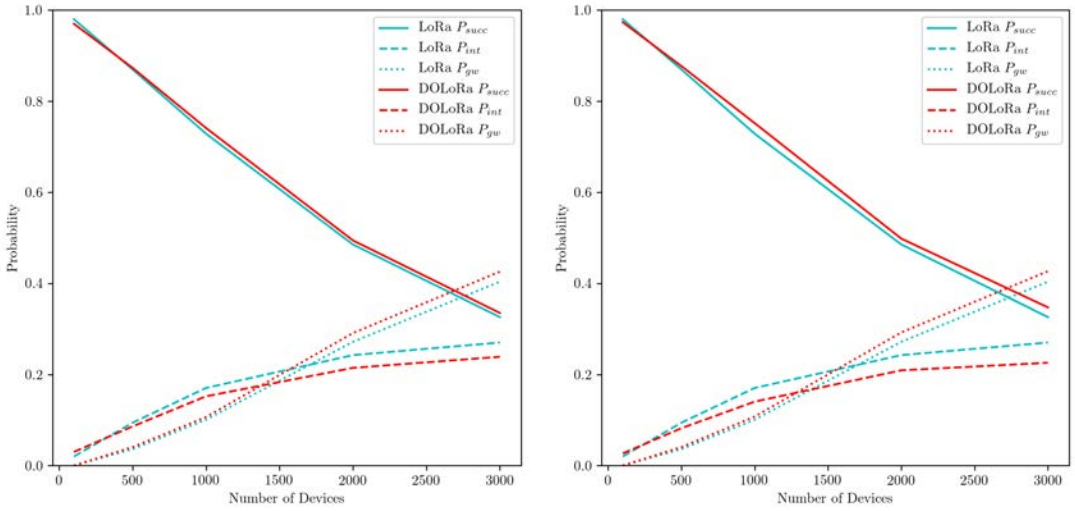

(a) Spreading factors are assigned to EDs through the *random approach*.

(b) Spreading factors are assigned to EDs through the *sensitivity approach*.

Figure 5.3: Statistical comparison between a LoRaWAN network employing only the standard LoRa modulation (in blue), and a LoRaWAN network that uses both the standard LoRa and the DOLoRa modulations (in red).

to the interference only if its power is grater than 3 dB of the colliding packet power. As a consequence if we assign the DOLoRa SF randomly it may happen that some packets will not respect the 3 dB margin and then they will be more likely to be destroyed. While if the DOLoRa SF are assigned according to the *sensitivity threshold*, chosen in such a way to guarantee the 3 dB guard margin in the SIR of the packets from different modulation schemes, we will never experience the previous phenomenon. In both the cases the results from the previous simulations are quite disappointing, in fact it seems that the new modulation doesn't provide any significant improvement in the performances of the LoRaWAN network, despite we are trying to get advantage of the pseudo-orthogonality between the spreading factors. The main problem is that the devices which are near to the gateway receive the lowest spreading factors, i.d. $SF = 7_1$ and $SF = 8_2$, and at the same time they continue to transmit packets with the maximum allowed power, i.e. $14dBm$, which means that they will destroy every other packet with the same spreading factor but a lower reception power. Moreover in the first ring of devices (the one associated to $SF = 7_1$ and $SF = 8_2$) there is a very high variance in the sensitivity received by the gateway, which corresponds to an higher probability of channel capture by stronger devices, even though they have

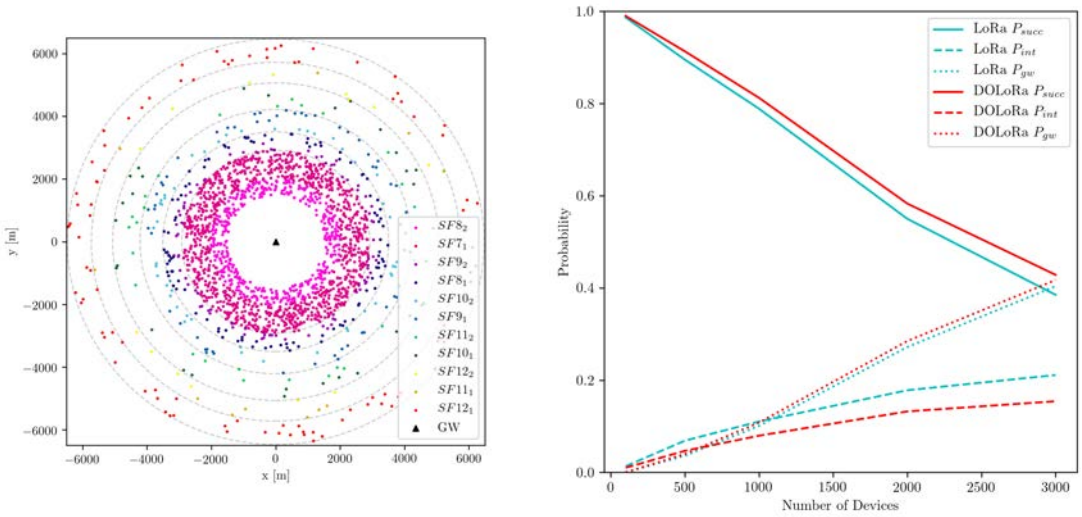

(a) The network topology of a LoRaWAN network with 2000 devices that uses both LoRa and DOLoRa modulations (sensitivity approach).

(b) Statistical description of the LoRaWAN network deployment in Figure 5.4a.

Figure 5.4: Results from the simulations with the implementation of a rudimental power control mechanism.

different spreading factors. The power gap can be much greater than the highest rejection threshold (which is 24 dB) in Table 5.5.

All these things together produced the previous equivocal results. Therefore to prove the advantages of the dual orthogonality modulation we performed another campaign of simulations where the devices where placed starting from a certain radius onward. This operation can be seen as a very rudimental way to reduce the transmitting power of the nodes near to the gateway.

In Figure 5.4a is shown an example of nodes deployment used for these simulations. Now we can see that the new modulation introduces a more noticeable improvement of the network performances (Figure 5.4b), in particular it is clear that when we use the DOLoRa modulation we must take into account the transmitting power of the end devices, which should be adapted with respect to the received power at the gateway.

Finally we remark that it is important to analyse the received power distribution of the EDs at the GW, before implementing any policy of power equalization when we assign the spreading factors to nodes. For example let's consider as a case of study a network of 2000 devices, that are using the standard LoRa mod-

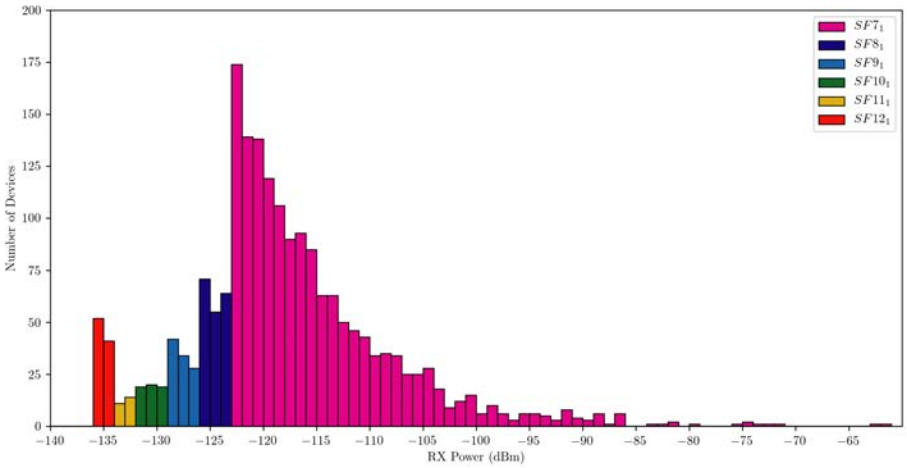

Figure 5.5: Received power distribution of 2000 devices. All devices are transmitting with the maximum allowed power: $14dBm$.

ulation. All the devices are transmitting at 14 dBm and are divided between the spreading factor according the distribution in [10]. As guessed, in Figure 5.5 we can see that the received power of the nodes with $SF = 7$ ranges from -60 dBm down to -124 dBm. Since this gap is quite large (around 65 dB) it may happen that some packets from the distant nodes will be destroyed by the stronger packet sent by the devices near the gateway. Then we can partially limit this phenomenon by reducing the power of the nearer devices, even though this might not be sufficient to have a reasonable increase in the network performances.

5.3 DLoRa (Decreasing LoRa)

The DLoRa (Decreasing LoRa) modulation is similar to the conventional Lora modulation and it is also compatible with it. DLoRa employees the same structure of the standard LoRa signal with the only difference that its instantaneous frequency is decreasing instead of increasing with time. In this section we will show that this new modulation will allow us to double the number of pseudo-orthogonal channels by using at the same time LoRa and DLoRa modulations, which will improve the network level performances of LoRa based networks.

5.3.1 Description of the modulation

The new set of downchirp signals that compose the DLoRa modulation is characterized by a decreasing instantaneous frequency. To build them we need to repeat the same argumentations of Section 3.1, with the only difference that the starting equation of the instantaneous frequency (3.5), should be modified as

$$f_D(t,a) = a\frac{B}{M} - \frac{B}{T_s}t + Bu(t-\tau'_a) - \frac{B}{2}, \quad 0 \leq t < T_s \tag{5.12}$$

where

$$\tau'_a = T_s\frac{a}{M} \tag{5.13}$$

Therefore we can obtain the phase through the integration of (5.12):

$$\begin{aligned}\Phi_D(t,a) &= 2\pi\int_0^t f_D(\tau,a)d\tau \\ &= 2\pi\left[a\frac{B}{M}t - \frac{B}{2T_s}t^2 + Btu(t-\tau'_a) - \frac{B}{2}t\right]\end{aligned} \tag{5.14}$$

which lead to the final equation of the DLoRa signals

$$x_D(t;a) = \exp\left\{j2\pi\left[a\frac{B}{M}t - \frac{B}{2T_s}t^2 + Btu(t-\tau'_a) - \frac{B}{2}t\right]\right\}, \quad 0 \leq t < T_s \tag{5.15}$$

This expression is valid for every symbol $a \in \{0,1,\ldots,M-1\}$. In Figure 5.6 we can see the characteristic frequency behaviour of the DLoRa signals compared to the one of a canonical LoRa signal. As for the standard LoRa modulation the discrete set of equation is obtained by sampling the continuous time equation of the DLoRa signals every $T = \frac{1}{B} = \frac{T_s}{M}$ seconds. So the discrete equation of DLoRa in the interval $[0, T_s[$ is

$$x_D(kT;a) = \exp\left\{j2\pi k\left[\frac{a}{M} - \frac{1}{2} - \frac{k}{2M}\right]\right\}, \qquad k = 0,1,...,M-1 \tag{5.16}$$

It is straightforward to show that the DLoRa modulation enjoys the same properties of the LoRa modulation, and in particular also the orthogonality between waveforms with different SF remains valid. It is as well straightforward to see that the demodulator structure of the DLoRa signals can be obtained using the

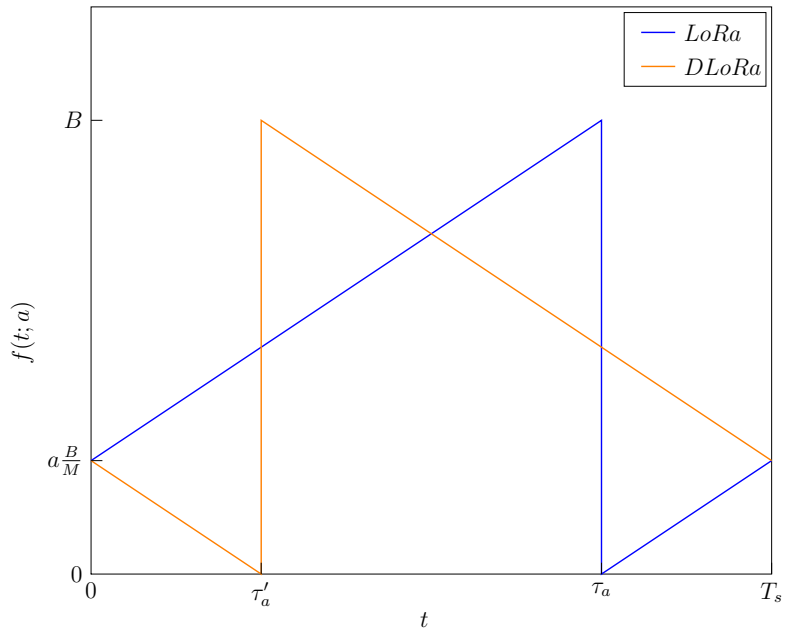

Figure 5.6: Frequency behaviour of one upchirp (blue) and one downchirp (orange) with symbol a.

same demodulator structure of the LoRa signals, just replacing a downchirp with an upchirp. As a consequence the dechirping term that we will need to use for the optimum efficient DLoRa demodulator is:

$$e^{\jmath 2\pi \frac{k^2}{2M} + \jmath \pi k} \tag{5.17}$$

The remaining part of the signal decoding does not change.

The combination of LoRa and DLoRa modulations can double the number of channels from 6 to 12, which enables a superior network level performance since the EDs can be assigned to twice the number of subchannels. The most relevant advantage is that the reduction of the collision probability is possible. The only constraint to achieve all this is to adopt some algorithms at network management level that assign the different SFs to the EDs, taking into account the SF pseudo-orthogonality and the channel capture effect. For example we can employ the latest and most promising "Capture Aware Sequential Watergilling Adaptive Data Rate" algorithm proposed in [40]. Finally in the vast majority of the ADR algorithm the availability of an higher number of channels (even though they are quasi orthogonal) is definitely beneficial. This is remarking how valuable

SF_r \ SF_i	7	8	9	10	11	12	7_D	8_D	9_D	10_D	11_D	12_D
7	0	-10	-12	-12	-13	-14	-11	-11	-11	-11	-12	-13
8	-12	0	-13	-14	-15	-16	-13	-14	-14	-14	-14	-15
9	-16	-15	0	-16	-17	-18	-15	-16	-16	-17	-17	-17
10	-18	-18	-18	0	-19	-20	-18	-18	-19	-19	-20	-20
11	-21	-21	-21	-21	0	-21	-21	-21	-21	-22	-22	-23
12	-23	-24	-24	-24	-24	0	-23	-24	-24	-24	-25	-25
7_D	-11	-11	-11	-11	-12	-13	0	-10	-12	-12	-13	-14
8_D	-13	-14	-14	-14	-14	-15	-12	0	-13	-14	-15	-16
9_D	-16	-16	-17	-17	-17	-17	-16	-15	0	-16	-17	-18
10_D	-18	-18	-19	-20	-20	-20	-18	-18	-18	0	-19	-20
11_D	-21	-21	-21	-22	-22	-23	-21	-21	-21	-21	0	-21
12_D	-23	-24	-24	-24	-25	-25	-23	-24	-24	-24	-24	0

Table 5.6: Thresholds on the SIR between the desired signal and the interferer signal in order to guarantee a $BER = 0.01$. The subscript indicate which are the SFs associated to DLoRa.

is to double the number of subchannels.

5.3.2 Simulations

First of all we compute the rejection thresholds for the DLoRa and LoRa modulations combined together, which are reported in Table 5.5. As we can notice from the values in the table, now we have 12 pseudo-orthogonal channels. Another important remark is that for every standard SF we have the equivalent DLoRa SF counterpart, that behaves in the same manner as the canonical version of it. In fact we can immediately see that the Table 5.6 values present symmetry: the values in the upper left part of the table (the one related to the standard LoRa modulation) form a square matrix that perfectly coincides with the square matrix, built in a similar way with the values in the lower right part of the table (the one related to the DLoRa modulation). The same reasoning is valid for the other two blocks on the upper right part of the table and in the lower left part of the table.

Now we are ready to investigate the performances of the new modulation in the real case scenario described in Section 5.1. As for the DOLoRa modulation, our target is to analyse how much the DLoRa modulation is able to improve the

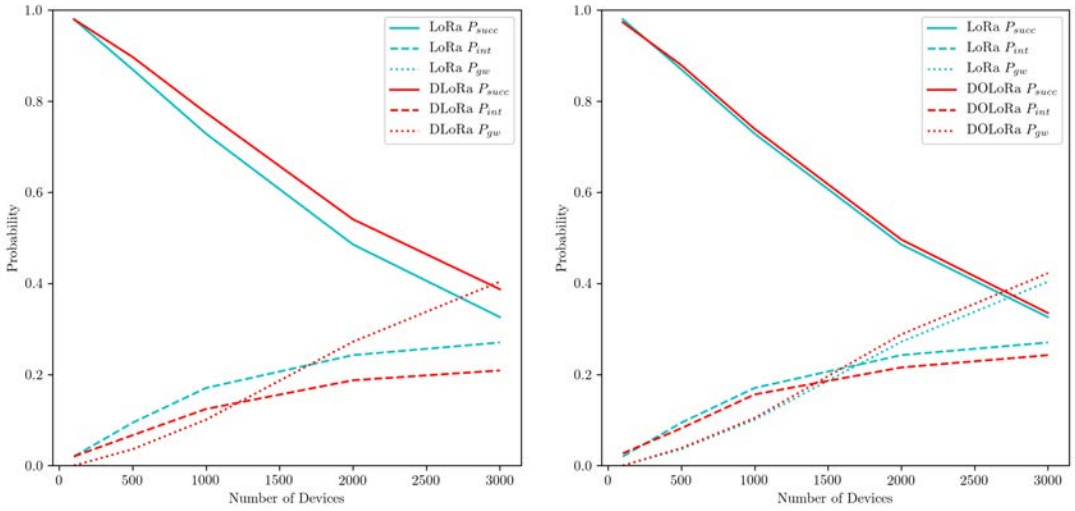

(a) Spreading factors are assigned to EDs through the *random approach*.

(b) Spreading factors are assigned to EDs through the *sensitivity approach*.

Figure 5.7: Statistical comparison between a LoRaWAN network employing only the standard LoRa modulation (in blue), and a LoRaWAN network that uses both the standard LoRa and the DLoRa modulations (in red).

probability to successfully transmit a PHY LoRa packet. This will be achieved through multiple simulations in scenarios with an increasing number of EDs inside the LoRaWAN network.

The simulation are performed into two different campaign and their results are shown in Figure 5.3. In the first campaign we have assigned the SF to the EDs by means of the *random approach* (Figure 5.7a), while in the second we used the *sensitivity approach* (Figure 5.7b). Now the approach that is performing better is the random approach, with which we can take advantage of the channel capture effect, as it is suggested in [40]. The sensitivity approach gives worse result because it reduces the variance of the received power of every SF and thus it reduces the chances to experience a channel capture. In other words with this last approach the LoRaWAN network has similar performances to a pure ALOHA system, where if we have two colliding packets they will be both destroyed by their interference, i.e. neither the two packets can be successfully demodulated and decoded. From the simulations in NS3 seems that the improvement introduced by DLoRa, at the LoRaWAN network level, are minimal, even though they are much more evident than the one produced by DOLoRa. Finally the main problem that is possibly hiding the real benefits of these two new modulations, and in

particular of DLoRa, is that we are not using an efficient algorithm to assign the SFs to the EDs. In fact a possible good ADR mechanism that we may implement in NS3 should take into account also the SF rejection thresholds between the SF of the EDs, and not only the reception power of the packets.

6
Conclusion

The purpose of this work was to introduce two new modulations DOLoRa and DLoRa with the aim at improving the network level performances of LoRaWAN.

After an introduction on the emerging paradigm of IoT, which is changing our everyday life by enabling the Internet connectivity of almost every object around us, we focused on the LPWAN technologies. In particular we described the peculiarities of NB-IoT, SigFox and Ingenu systems.

Then we covered the LoRa modulation and the LoRaWAN systems, with a special attention for derivation of the LoRa analytical equations both in the continuous and discrete time domain. In fact this was a necessary key point to better understand the DLoRa modulation design. Moreover these equations were also useful to obtain the properties of the LoRa waveforms, which are at the basis of the DOLoRa modulation.

In Chapter 3 we have also described the optimum LoRa receiver and also an efficient implementation of it, that involves the characteristic LoRa dechirping procedure.

At this point we discussed the pseudo-orthogonality of the Spreading Factors, which is a very active and controversary topic in the LoRa literature. In fact in literature there so many different opinions specifically in the quantification of the spreading factors orthogonality margins, that are usually expressed in terms of Signal-to-Interference ratio or in terms of signal-to-Interference-plus-Noise ratio.

Therefore we described the MATLAB simulator that we have created to compute the spreading factors rejection thresholds, whose values are in accordance to the more accredited SIR margin available in literature. This MATLAB simulator is of fundamental importance since it has been used to compute the thresholds on the pseudo-orthogonality of the standard LoRa Spreading Factors against the one from the new modulations.

In the last part of the thesis DOLoRa and DLoRa are described from an analytical point of view and then are summarized all the benefits that the two modulations can bring to the LoRaWAN networks.

Finally all the theoretical part of DOLoRa and DLoRa is tested and verified through some simulations in NS3, carried out in a real case scenario, where there is an unbalanced use of the spreading factors. Even though the improvement in these simulation can appear marginal, it should be noted that our simulations are lacking of a good Adaptive Data Rate algorithm.

6.1 Future work

As future work an innovative Adaptive Data Rate algorithm should be implemented in such a way to take a real advantage of the DOLoRa and DLoRa modulations. In particular the ADR should take into account the pseudo-orthogonality of the spreading factors, and find out a technique to distribute the spreading factors while exploiting the benefits of the channel capture effects. Another fundamental aspect that should be considered by the ADR is the power control mechanism. More specifically we need to address the problem of the end devices near the gateway, whose packets are received with a very high power, even though the nodes are transmitting with the lowest allowed power by the LoRaWAN protocol.

Finally it will be also interesting to investigate the behaviour of the LoRaWAN networks that are using in the underlying physical layer a combination of LoRa, DOLoRa and DLoRa modulations.

Bibliography

[1] C. Goursaud and J. M. Gorce, "Dedicated networks for IoT: PHY / MAC state of the art and challenges," *EAI Endorsed Transactions on Internet of Things*, vol. 1, no. 1, p. 150597, 2015.

[2] Semtech Corporation, "SX1272/3/6/7/8 LoRa Modem Design Guide," no. July, p. 9, 2013. [Online]. Available: https://www.semtech.com/uploads/documents/LoraDesignGuide{_}STD.pdf

[3] M. Centenaro, L. Vangelista, A. Zanella, and M. Zorzi, "Long-range communications in unlicensed bands: The rising stars in the IoT and smart city scenarios," *IEEE Wireless Communications*, 2016.

[4] LoRa Alliance, "LoRaWAN 1.1 Specification," *Lora Alliance*, no. 1.1, p. 101, 2017. [Online]. Available: https://lora-alliance.org/sites/default/files/2018-04/lorawantm{_}specification{_}-v1.1.pdf

[5] LoRa Alliance, "LoRaWAN Backend Interfaces 1.0.4 Specification," *LoRa Alliance*, no. 2010, p. 97331, 2017. [Online]. Available: https://lora-alliance.org/sites/default/files/2018-04/lorawantm-backend-interfaces-v1.0.pdf

[6] M. Knight and B. Seeber, "Decoding LoRa: Realizing a Modern LPWAN with SDR," *Wuli Xuebao/Acta Physica Sinica*, 2011.

[7] D. Magrin, M. Centenaro, and L. Vangelista, "Performance evaluation of LoRa networks in a smart city scenario," in *IEEE International Conference on Communications*, 2017.

[8] Lora Alliance, "LoRaWAN 1.1 Regional Parameters," *Lora Alliance*, pp. 1–56, 2017. [Online]. Available: https://lora-alliance.org/sites/default/files/2018-07/lorawan{_}regional{_}parameters{_}v1.0.3reva{_}0.pdf

[9] Semtech Corporation, "SX1301 Datasheet," no. June, pp. 1–40, 2017. [Online]. Available: https://semtech.my.salesforce.com/sfc/p/

{#}E0000000JelG/a/44000000MDnR/Et1KWLCuNDI6MDagfSPAvqqp.Y869Flgs1LleWyfjDY

[10] L. Vangelista, L. Dell'Anna, and P. Palazzzoli, "A battery lifetime comparison between LoraWAN and Wireless MBus smart meters," in *2019 IEEE International Black Sea Conference on Communications and Networking (BlackSeaCom)*. IEEE, 2019.

[11] A. Zanella, N. Bui, A. Castellani, L. Vangelista, and M. Zorzi, "Internet of things for smart cities," *IEEE Internet of Things Journal*, 2014.

[12] J. Gubbi, R. Buyya, S. Marusic, and M. Palaniswami, "Internet of Things (IoT): A vision, architectural elements, and future directions," *Future Generation Computer Systems*, 2013.

[13] P. Bellavista, G. Cardone, A. Corradi, and L. Foschini, "Convergence of MANET and WSN in IoT urban scenarios," *IEEE Sensors Journal*, 2013.

[14] Department Statista Research, "Internet of Things (IoT) connected devices installed base worldwide from 2015 to 2025," 2019. [Online]. Available: https://www.statista.com/statistics/471264/iot-number-of-connected-devices-worldwide/

[15] R. S. Sinha, Y. Wei, and S. H. Hwang, "A survey on LPWA technology: LoRa and NB-IoT," *ICT Express*, vol. 3, no. 1, pp. 14–21, 2017. [Online]. Available: http://dx.doi.org/10.1016/j.icte.2017.03.004

[16] L. Vangelista, "Frequency Shift Chirp Modulation: The LoRa Modulation," *IEEE Signal Processing Letters*, 2017.

[17] M. Chiani and A. Elzanaty, "On the LoRa Modulation for IoT: Waveform Properties and Spectral Analysis," *IEEE Internet of Things Journal*, 2019.

[18] M. Centenaro, L. Vangelista, and R. Kohno, "On the impact of downlink feedback on LoRa performance," in *IEEE International Symposium on Personal, Indoor and Mobile Radio Communications, PIMRC*, 2018.

[19] L. Vangelista and A. Cattapan, "A new LoRa-compatible modulation improving the LoRaWAN network level performance," in *2019 IEEE Latin-American Conference on Communications (LATINCOM)*. IEEE, 2020.

[20] NS3, "The ns-3 network simulator," 2019. [Online]. Available: https://www.nsnam.org/

[21] 3GPP, "LTE Release 13," 2014.

[22] C. B. Mwakwata, H. Malik, M. M. Alam, Y. L. Moullec, S. Parand, and S. Mumtaz, "Narrowband internet of things (NB-IoT): From physical (PHY) and media access control (MAC) layers perspectives," *Sensors (Switzerland)*, vol. 19, no. 11, pp. 1–34, 2019.

[23] F. Sforza, "Communication system," *US 8.406.275 B2*, vol. 2, no. 12, 2013.

[24] A. Goldsmith, *Wireless communications*. Cambridge University Press., 2005.

[25] P. Robyns, P. Quax, W. Lamotte, and W. Thenaers, "A multi-channel software decoder for the LoRa modulation scheme," in *IoTBDS 2018 - Proceedings of the 3rd International Conference on Internet of Things, Big Data and Security*, 2018.

[26] D. Bankov, E. Khorov, and A. Lyakhov, "On the limits of LoRaWAN channel access," *Proceedings - 2016 International Conference on Engineering and Telecommunication, EnT 2016*, no. October 2017, pp. 10–14, 2017.

[27] D. Croce, M. Gucciardo, S. Mangione, G. Santaromita, and I. Tinnirello, "Impact of LoRa Imperfect Orthogonality: Analysis of Link-Level Performance," *IEEE Communications Letters*, vol. 22, no. 4, pp. 796–799, 2018.

[28] M. Bor, U. Roedig, T. Voigt, and J. M. Alonso, "Do LoRa low-power wide-area networks scale?" in *MSWiM 2016 - Proceedings of the 19th ACM International Conference on Modeling, Analysis and Simulation of Wireless and Mobile Systems*, 2016.

[29] ETSI, "Electromagnetic compatibility and Radio spectrum Matters (ERM); Short Range Devices (SRD); Radio equipment to be used in the 25 MHz to 1 000 MHz frequency range with power levels ranging up to 500 mW," pp. 1–73, 2012.

[30] CEPT, "ERC Recommendation 70-03," pp. 1–78, 2019. [Online]. Available: https://www.ecodocdb.dk/download/25c41779-cd6e/Rec7003e.pdf

[31] T. Elshabrawy and J. Robert, "Closed-Form Approximation of LoRa Modulation BER Performance," *IEEE Communications Letters*, 2018.

[32] N. Benvenuto and M. Zorzi, *Principles of Communications Networks and Systems*. Wiley, 2011.

[33] T. Elshabrawy and J. Robert, "Capacity Planning of LoRa Networks with Joint Noise-Limited and Interference-Limited Coverage Considerations," *IEEE Sensors Journal*, 2019.

[34] A. Mahmood, E. Sisinni, L. Guntupalli, R. Rondon, S. A. Hassan, and M. Gidlund, "Scalability Analysis of a LoRa Network under Imperfect Orthogonality," *IEEE Transactions on Industrial Informatics*, vol. 15, no. 3, pp. 1425–1436, 2019.

[35] D. Croce, M. Gucciardo, S. Mangione, G. Santaromita, and I. Tinnirello, "LoRa Technology Demystified: from Link Behavior to Cell Capacity," *IEEE Transactions on Wireless Communications*, 2019.

[36] J. Y. L. Boudec, *Performance evaluation of computer and communication systems*. EPFL Press, 2011.

[37] D. Magrin, M. Capuzzo, S. Romagnolo, and M. Luvisotto, "LoRaWAN NS3 module," 2019. [Online]. Available: https://github.com/signetlabdei/lorawan

[38] D. Magrin, "SEM Python Module," 2019. [Online]. Available: https://github.com/signetlabdei/sem

[39] S. Li, U. Raza, and A. Khan, "How Agile is the Adaptive Data Rate Mechanism of LoRaWAN?" in *2018 IEEE Global Communications Conference, GLOBECOM 2018 - Proceedings*, 2018.

[40] G. Bianchi, F. Cuomo, D. Garlisi, and I. Tinnirello, "Capture Aware Sequential Waterfilling for LoraWAN Adaptive Data Rate," *CoRR*, 2019. [Online]. Available: http://arxiv.org/abs/1907.12360